Role of road network for prevention and mitigation of runoff-induced geo-disaster under climate change

Tatsuya ISHIKAWA, Professor, Dr.Eng.
Faculty of Engineering, Hokkaido University
Kita 13, Nishi 8, Kita-Ku, Sapporo 060-8628, Japan
Tel: +81-11-706-6202, Fax: +81-11-706-6202
E-mail: t-ishika@eng.hokudai.ac.jp

Tingyong ZHANG, ex Master Course Student.
Graduate School of Engineering, Hokkaido University
Kita 13, Nishi 8, Kita-Ku, Sapporo 060-8628, Japan
Tel: +81-11-706-6203, Fax: +81-11-706-6203
E-mail: tingyong.zhang.m8@elms.hokudai.ac.jp

Wentao HE, ex Master Course Student.
Graduate School of Engineering, Hokkaido University
Kita 13, Nishi 8, Kita-Ku, Sapporo 060-8628, Japan
Tel: +81-11-706-6203, Fax: +81-11-706-6203
E-mail: wentao.he.h2@elms.hokudai.ac.jp

Yulong ZHU, Assistant Professor.
School of Water Resources and Hydropower Engineering, North China Electric Power University, Beijing 102206, China
E-mail: zhuyulong@ncepu.edu.cn

Shima KAWAMURA, Professor, Dr.Eng.
Department of Civil Engineering and Architecture, Muroran Institute of Technology
27-1, Mizumoto-cho, Muroran 050-8585, Japan
Tel: +81-143-46-5281, Fax: +81-143-46-5283
E-mail: skawamur@muroran-it.ac.jp

Role of road network for prevention and mitigation of runoff-induced geo-disaster under climate change

Tatsuya ISHIKAWA[*], Tingyong ZHANG[**], Wentao HE[**], Yulong ZHU[***], and Shima KAWAMURA[****]

[*] Faculty of Engineering, Hokkaido University
[**] ex Graduate School of Engineering, Hokkaido University
[***] School of Water Resources and Hydropower Engineering, North China Electric Power University
[****] Department of Civil Engineering and Architecture, Muroran Institute of Technology

Abstract. Under the climate change in recent years, heavy rainfalls that break observation records almost every year around the world have caused various geo-disasters. In particular, the frequent occurrence of torrential rainfall induced geo-disasters is accompanied by an increase in water-soil complex disasters caused by surface and seepage flows. For example, it has been reported in Japan that a large amount of rainwater, which cannot infiltrate into the soil ground, flows down the paved surface as a water channel, eroding and collapsing the natural slopes, embankments and cut slopes at the downstream. The Intergovernmental Panel on Climate Change (IPCC) forecasts that both the frequency of torrential rainfall and the amount of rainfall will continue to increase as extreme weather events become more frequent in the future. For this reason, there is a high possibility that record-breaking torrential rainfall will be observed, and that slope disasters at the unexpected locations along roads, which differ from the conventional mechanisms of slope failures, will emerge due to surface and seepage flows. Therefore, this study introduces a wide-area slope stability analysis considering rainfall infiltration and runoff useful for the risk assessment of water-soil complex landslide disasters with torrential rainfalls, which are expected to increase in various parts of the world in the future. In the end, based on case studies of actual geo-disasters with the proposed analysis, this study clarifies the perspectives necessary for the risk assessment of transportation infrastructures such as a road pavement, which is the outflow path of surface flow, and the disaster prevention and mitigation measures, and explain the role of road network as a linear structure under the climate change.

Keywords: Surface flow, Subsurface flow, Slope stability, Heavy rainfall, Coupled analysis

INTRODUCTION

Under the climate change in recent years, heavy rainfalls that break the observation records have caused serious geo-disasters around the world. The Intergovernmental Panel on Climate Change (IPCC) forecasts that both the frequency of torrential rainfall and the amount of rainfall will continue to increase as extreme weather events become more frequent in the future. In various parts of Japan, record-breaking heavy rainfalls are often causing various kinds of geo-disasters such as levee breach, large-scale slope failures, and debris flows almost every year. Even in Hokkaido, the northern island of Japan, where rainfall amount is traditionally low, heavy rainfalls are frequently being observed, increasing the risk of wide-area severe geo-disasters. According to the future climate forecast by the Ministry of Land, Infrastructure, Transport and Tourism in Japan, the maximum precipitation at the end of this century, is expected to be more than 1.4 times the current amount of rainfall in many areas of Hokkaido, though the national average is expected to be more than 1.3 times. This means that the high-latitude cold regions such as Hokkaido will experience more vulnerable to climate change than warmer regions such as Kyushu, the southern island of Japan, in the future.

Due to recent climate change, it is said that the global warming will induce an increase in the number of short-term heavy rainfall events with rainfall intensity of over 30 mm/h and the total amount of precipitation in a single rainfall event. In response to frequent short-term torrential rainfalls these days, a new type of slope failure mechanism has become apparent. In particular, the water/soil complex disasters (Figure 1) caused by surface and seepage flows during torrential rainfall are increasing. For example, it is reported in the heavy rainfalls in Hokkaido, 2016 and in Kyushu, 2020 that a large amount of rainwater, which cannot infiltrate into soil ground, flows down the paved road surface as a water channel, caused surface flow to erode and collapse natural slopes, embankments and cut slopes at the downstream (JGS, 2017; Mukunoki, et al., 2021). In addition, there are some cases where it is suspected that a rainfall exceeding the drainage capacity of earth structures results in a large amount of groundwater and surface water, causing a blockage of drainage ditches and culverts, or an overflow due to excess flow, and finally inducing slope failures.

(a) Geotechnical disasters in Hokkaido, Japan induced by heavy rainfall on August, 2016

(b) Geotechnical disasters in Kyushu, Japan induced by heavy rainfall on July, 2020
(provided by Prof. Sako, Kagoshima University, and Kagoshima Pref.)

Fig. 1 Rainfall triggered catastrophic landslides in Japan.

Besides, Hokkaido has been less affected by typhoons and heavy rainfalls and has experienced fewer rainfall induced geo-disasters compared to other regions in Japan, so many areas of Hokkaido is not accustomed to rainfall and landslides. For this reason, the rainfall threshold for landslides in Hokkaido is smaller as compared with those in other regions in Japan, and in case of heavy rainfall, the geo-disasters are likely to occur. Furthermore, there are concerns that the damaged area expands, and that the damage degree becomes more serious as shown in Figure 2. Therefore, in case record-breaking heavy rainfall will be observed in the near future, there is a high possibility that landslide disasters at the unexpected locations along roads, which differ from the conventional mechanisms of slope failures, will emerge due to surface and seepage flows. However, the water/soil complex landslide disasters caused by surface flows and seepage flows along the road network, which are expected to increase in various parts of the world in the future, have not been sufficiently studied in terms of geotechnical engineering.

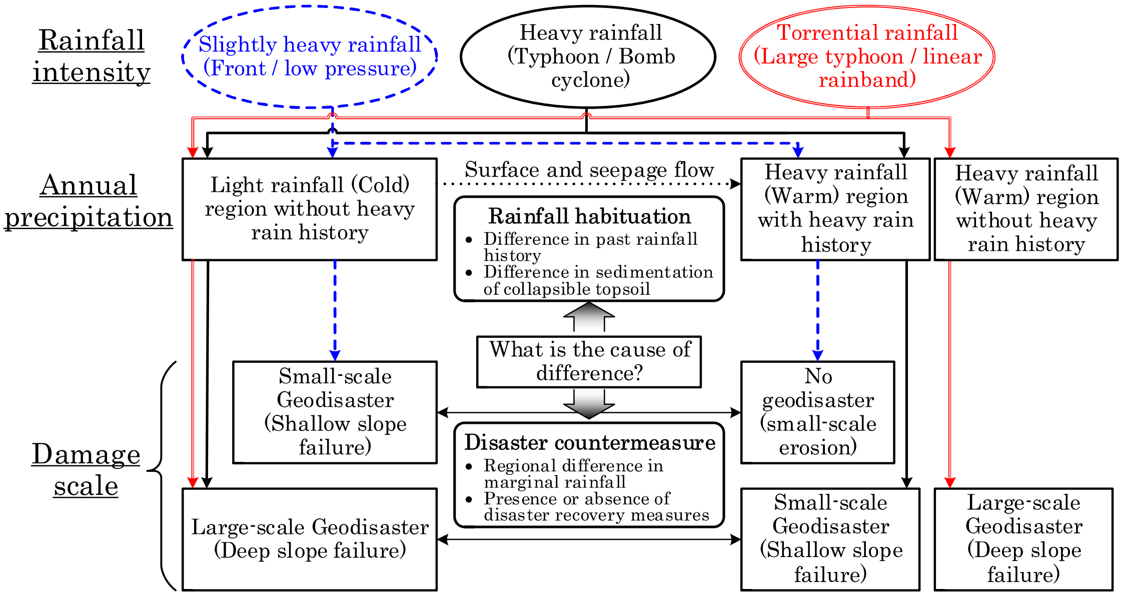

Fig. 2 Influence of rainfall habituation on ground behavior.

Considering the above background, this study introduces a wide-area (e.g. 1 km × 1 km) slope stability analysis considering rainfall infiltration and runoff, which is useful for the risk assessment of water/soil complex landslide disasters during torrential rainfalls. Next, through reproduction analysis of two actual landslide disasters, this study outlines the effects of the material properties and the shape characteristics of topography and structures in a three-dimensional (3D) analytical model on the simulation results and examines the applicability of the proposed numerical simulation to the practical use. Finally, this study clarifies the perspectives necessary for the risk assessment of transportation infrastructures such as road pavement, which is the outflow path of surface flow, and the disaster prevention and mitigation measures, and explain the role of road network as a linear structure under the climate change.

LITERATURE REVIEW

Slope Stability Assessment Methods

The Limit Equilibrium Method (LEM) is commonly employed in the slope stability analysis because of their proven effectiveness and reliability (Bishop, 1955; Janbu, 1968; Morgenstern and Price, 1965). In the LEM, the geometry and/or the location of the potential failure surfaces are approximated, and the mass of a potential failure slope is discretized into smaller vertical slices. By assuming that each slice is considered as a unique sliding block and the shear strength is mobilized with the same ratio of shear stress to shear strength for all slices, and applying the principles of force and/or moment equilibrium, the LEM seeks an indicator of slope stability, namely "Factor of Safety (FOS)", which is typically defined as the ratio of the resisting forces (shear strength) to the driving forces (shear stress) required for equilibrium along the prescribed failure surface. Depending on how interslice forces in shear and normal directions, and total stress and pore water pressure are handled, and the equilibrium principles of forces and moments are involved, many variations of limit-equilibrium methods have been proposed. However, the determination of where the failure initiates or the ultimate geometry and position of a failure surface is one of the fundamental challenges when using LEM.

In addition, the Shear Strength Reduction Technique (SSRT) is also usually applied in the slope stability analysis (Matsui and San, 1992). An important characteristic in this method is that the slope failure is defined according to the shear strain failure criterion such as Mohr–Coulomb model and similar material model. Unlike the LEM, no assumptions need to be made about the location or shape of the failure surface, and the interslice forces on the sides of the slices and their directions when using the SSRT. Besides, the critical failure mechanism in a complicated model may assume any shape. In the SSRT, the failure of slope is defined as that the failure shear strain develops from the toe to the top of the slope by reducing the strength parameters (cohesion and internal friction angle) of the soil until the slope becomes unstable. The FOS is defined as the ratio of the real shear strength to the reduced shear strength of the soil. In the numerical simulation, the shear strength reduction factor just before analysis cannot converge within a user-specified number of iterations is considered as the FOS of the slope. This will allow the users to assess the local instability of specific parts of the model as well as the total instability of the entire model.

However, it is worth noting that the LEM and SSRT are effective for the stability analysis of a single slope but not feasible for the stability analysis of multi slopes on a catchment-scale. Lu et al. (2012) proposed an approach, i.e. the Local Factor of Safety (LFS) approach to quantify the FOS of a slope under rainwater infiltration and verified that the assessment of the LFS approach is consistent with the LEM. Furthermore, the LFS approach has the potential to overcome several major limitations in the classical FOS methodologies, such as the initiation and evolution of instability with changes in pore water pressure, and the inherent underestimation of slope instability (Lu et al., 2012). The LFS approach also has the potential to evaluate the slope instabilities on a catchment-scale.

Coupled Surface and Subsurface Flow Model

In the conventional assessments for rainfall-induced slope instability, the impact of surface runoff is often neglected to simplify calculations. However, in reality, the surface runoff plays a significant role in slope stability, particularly in areas with varying topography and drainage patterns as some disaster investigation reports mentioned. For example, the surface runoff is generated by the catchment topography and drains out from high elevation to concave situation. Then, the road embankment crossing the gully position where the runoff water is gathered may suffer a high risk of slope failure during heavy rainfall. To figure out the runoff-induced landslide mechanism and accurately assess the effect of surface flow on slope instability, over the last decades, there has been various research focused on understanding the complex interactions between surface and subsurface flows, and the mechanisms leading to surface runoff. Several earlier studies made attempts to develop models that can describe the behavior of surface flow. Some of these models involve solving shallow water equations using the finite-difference method, which accurately tracks surface flow and provides water depth and velocity information at specific points (Esteves et al., 2000). Meanwhile, in order to simplify runoff simulations and improve computational efficiency, the kinematic and diffusive wave approximations based on shallow water equation simplifications have been commonly used for runoff simulations (Tseng, 2010; Mügler et al., 2011; Zhu et al., 2020). For estimating the soil infiltration capacity of surface ground, important for calculating the timing of runoff or ponding generation (i.e. when the rainfall intensity exceeds the soil infiltration capacity, runoff generates along the ground), successful infiltration models such as Green-Ampt model and Horton model have been employed (Green and Ampt, 1911; Horton, 1933; Simons et al., 2014). Rainwater infiltration involves two stages (Tan et al., 2018): rainfall infiltration stage during the light rainfall or in the early stage of heavy rainfall without any runoff generation where raindrops directly infiltrate into the soil after reaching the ground surface, and runoff infiltration stage in the later stage of heavy rainfall with runoff generation where part of runoff from the upstream infiltrates into the soil, and the rest flows downstream with rainwater. In addition, to describe water flow in unsaturated soil in the vadose zone, the Richards model is used, which combines the continuity equation with Darcy's law to form a partial differential equation (PDE) for unsaturated soil water flow. Various numerical methods such as the finite-element or finite-difference methods have been used to solve the highly nonlinear Richard's equation (Clement et al., 1994; Belfort et al., 2013). However, there is currently a gap in research as there are no simplified methods or numerical models available to simultaneously simulate coupled surface and subsurface flow during heavy rainfall while also considering slope stability. This area calls for further research and development to better understand and model the complex interactions between surface and subsurface flow in such conditions.

EXAMPLES OF RAINFALL-INDUCED SLOPE FAILURES

Geo-disasters in Nissho Pass Area on August 2016 Hokkaido Heavy Rainfall

In 2016, Typhoon No.10 (Lionrock) brought a record-breaking heavy rainfall in Tokachi region of Hokkaido, Japan during August 29 to 31, which resulted in the most serious geo-disaster ever reported in Hokkaido affecting wide areas of the Hidaka Mountains. In particular, extremely heavy rainfall was observed at the 7th stage or higher of the Nissho Pass along the National Highway Route 274, thus causing considerably damaged due to landslides, embankment collapses, and debris flows. According to the observations (Figure 3) at the nearest meteorological telemetry station, namely Nissho Pass TeleMeter (TM) located at the mountaintop, the cumulative rainfall that fell from 19:00 on August 28th to 10:00 on August 31st was 488 mm with the maximum hourly rainfall of 55 mm at 01:00 on August 31st and the maximum Soil Water Index (SWI) of 278 mm, which is the highest rainfall ever recorded in the Nissho Pass area. Figure 4 shows two large-scale embankment collapses that occurred close to each other near the 7th stage on August 31. The scale of Location 1 slope failure was approximately 80 to 100 m wide, 40 to 50 m long, 10 to 15 m thick, with a collapsed soil volume of 15,300 m^3 and a slope angle of 32°. The road significantly collapsed at the curved part, and the road body was largely damaged. During the investigation (JGS, 2017), there were traces of a large amount of surface water and debris flow on the pavement surface flowing down from the higher 8th stage direction. This indicates that both erosion and scour induced by the surface flow can cause a large-scale collapse at the top of the embankment slope where the road alignment changes from a straight line to a curve. The granite that is more weathered at the shallower parts of subsurface layer owing to climate conditions deposits over the sedimentary rocks in the Hidaka belt, and the upper part of the weathered granite is covered by periglacial slope deposits mixed with gravel. The extra heavy rainfall observed at the 7th stage or higher caused a large amount of rainwater to infiltrate into the soil ground that comprised a fine-grained weathered granite "Masado", thereby weakening the soil ground and inducing the slope failures. Owing to these considerable damages, the National Highway Route 274 was closed for approximately one year from August 30, 2016 (when the road was closed before geo-disaster struck) to October 29, 2017 (when the restoration was completed).

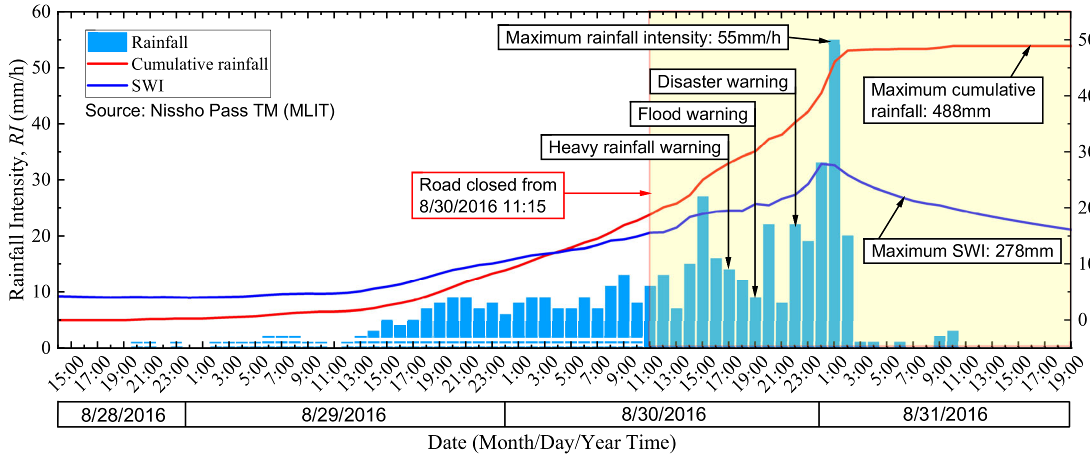

Fig. 3 Rainfall recorded during Typhoon No.10 at Nissho Pass TM.

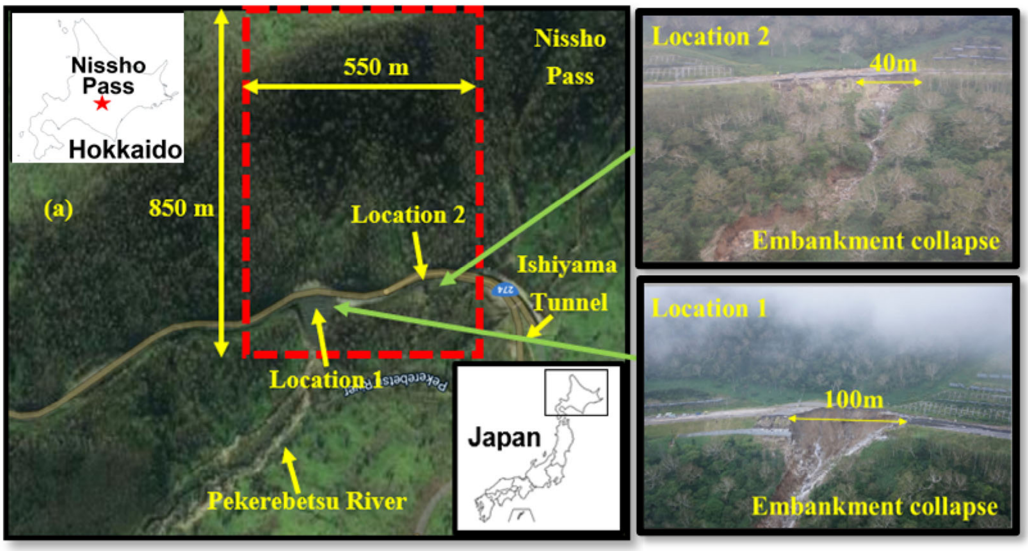

Fig. 4 Geo-disasters at the 7th stage of Nissho Pass on August 2016 Hokkaido Heavy Rainfall.

Geo-disasters in Shikotsu Lake Area on September 2018 Hokkaido Eastern Iburi Earthquake

On September 5, 2018, the day before the 2018 Hokkaido Eastern Iburi Earthquake, a slope failure occurred on a natural slope along the National Highway Route 453 near Shikotsu Lake (Figure 5b, hereafter referred to as "Case 1"). The scale of Case 1 slope failure was 20 m wide, 120 m long, 0.5 to 1 m thick, with a collapsed soil volume of 1,800 m^3 and a slope angle of more than 50°. The Eniwa Falling Pumice layer (presumed to be a secondary deposit) was deposited on top of the mudstone (shale), and the slip occurred in this layer. The collapsed soil and fallen trees overcame a rockfall protection fence and reached the Shikotsu Lake. The post-collapse slope was reported to have exposed the Eniwa Falling Pumice layer, and no clear spring was observed on the slope (JGS, 2019). As shown in Figure 6, the heavy rainfall with the cumulative rainfall of 263 mm, the maximum hourly rainfall of 51 mm, and the maximum soil water index of 187 mm were recorded at the nearby Kita Oku Izari TM (located 7 km away) from September 3rd to 5th 2018, which triggered the slope failure of Case 1.

On the other hand, along the same route where Case 1 slope failure occurred, on the day of the earthquake (occurred at 3:07 a.m. on September 6, 2018), another slope failure occurred on a cut slope with the Eniwa Falling Pumice layer similar to Case 1 as the slip surface (Figure 5c, hereafter referred to as "Case 2"). Case 2 is located approximately 1.6 km west of Case 1. The scale of the

Case 2 slope failure was 40 m wide, 60 m long, 2 m thick, with a collapsed soil volume of 4,800 m^3. The slope failure occurred on a steep slope of approximately 50°. The collapsed soil overcame a concrete retaining wall (3 m high) with a rockfall protection fence and reached the slope on the opposite side. The collapsed soil with the volume of 2,100 m^3 had accumulated on the road surface over an area of 11.5 m wide, 47 m long, and 4 m thick on average. The Eniwa Falling Pumice layer was exposed, and no clear spring was observed on the slope after the collapse. As shown in Figure 7, the strong seismic motion with the JMA seismic intensity of lower 6 was observed, and the maximum acceleration of 559.4 Gal, 384.1 Gal and 325.3 Gal on EW, NS and UD directions were respectively recorded at the nearby Shikotsu Lake seismic station (HKD185). The strong seismic motion should play a significant role in the slope failure of Case 2 since earthquake took place just before the collapse. Meanwhile, it is considered that the heavy rainfall occurred before slope failure of Case 2 should also be one of exogenous factors of slope failure though it is unclear which has a greater influence, earthquake or rainfall.

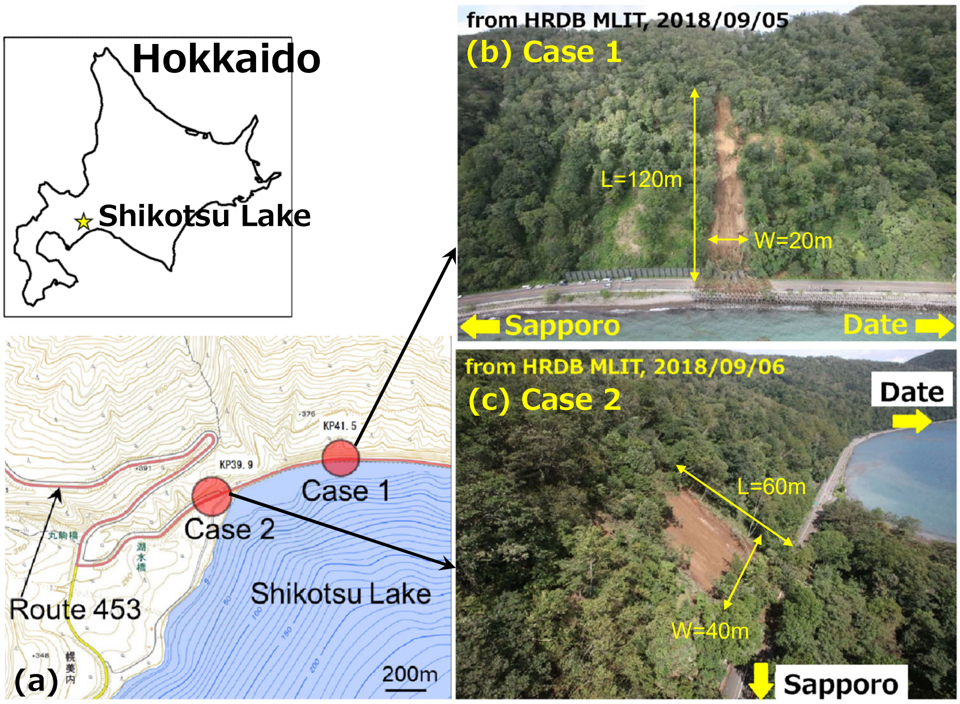

Fig. 5 Geo-disasters in Shikotsu Lake area on September 2018 Hokkaido Eastern Iburi Earthquake.

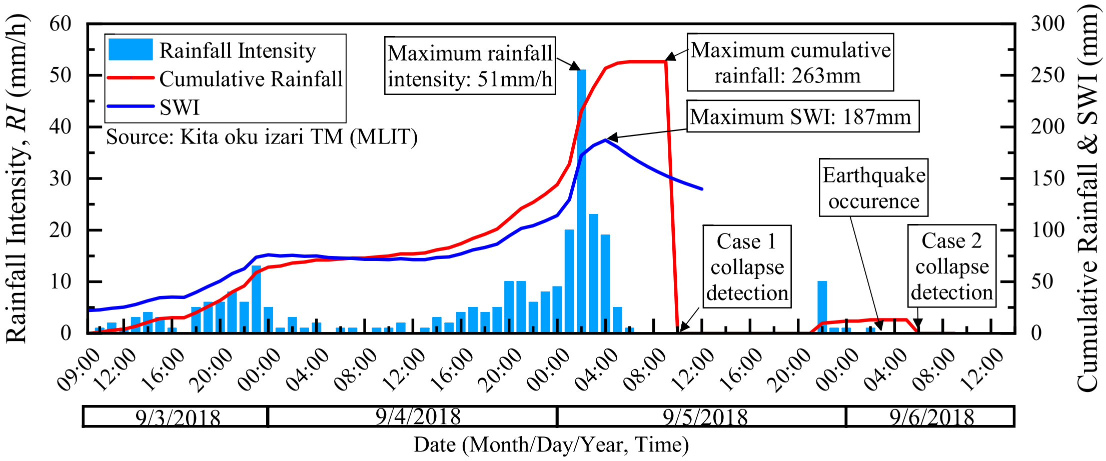

Fig. 6 Rainfall recorded before 2018 Hokkaido Eastern Iburi Earthquake at Kita oku izari TM.

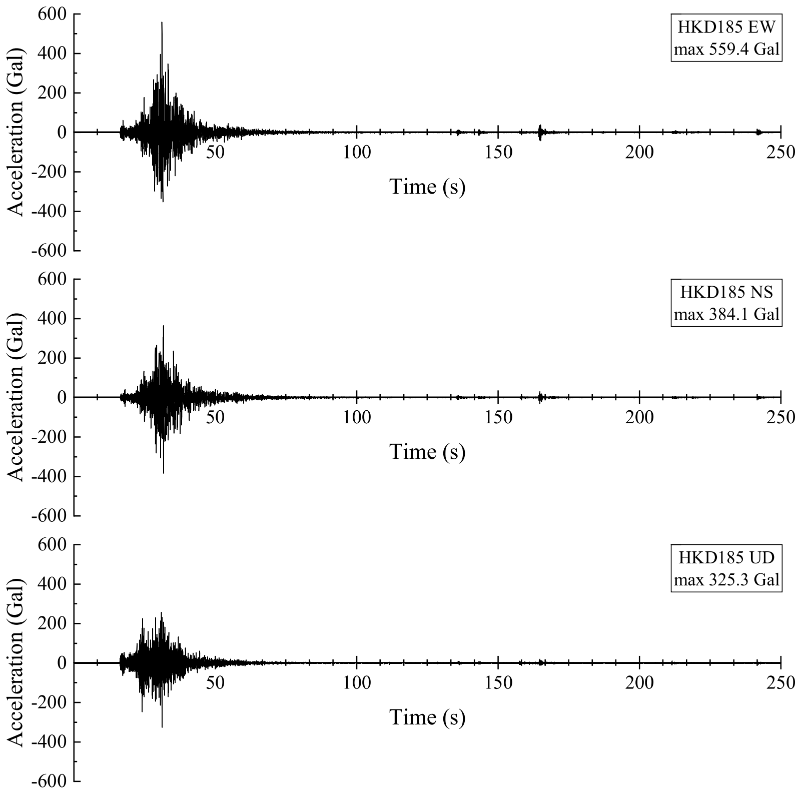

Fig. 7 Acceleration waveforms recorded at 2018 Hokkaido Eastern Iburi Earthquake at Shikotsu Lake seismic station (HKD185).

NUMERICAL SIMULATION METHOD

Slope Stability Analysis with Coupled Surface and Subsurface Flow

To evaluate the stability of multi slopes against the water/soil complex landslide disasters during torrential rainfalls on a catchment-scale considering the complex interactions between surface flow and subsurface flow, a hybrid coupled model using the Finite Element Method (FEM) software COMSOL (COMSOL Multiphysics, 2018), which was proposed by Zhu et al. (2020) and later modified by He et al. (2023), is employed in this study. The model integrates surface flow, subsurface flow, and soil mechanics through bidirectional and unidirectional coupling processes. This comprehensive approach allows for the simulation of the runoff, infiltration, seepage, and slope instabilities on both wide and narrow area to accurately release warning information to the dangerous spots in the target region. The model comprises two components: hydraulic component and mechanical component. Firstly, in the hydraulic component, the two-dimensional (2D) surface flow model based on the Diffusion wave equation and 3D subsurface flow model using the Richards's equation are established by the PDE module in COMSOL to calculate the distribution of runoff depth and velocity on the terrain surface, along with the distribution of pore water pressure and volumetric water content in the soil ground. The surface and subsurface flow models are bidirectionally coupled through infiltration and exfiltration. For example, the water depth calculated from the surface flow model is applied to the subsurface flow model as the water head boundary condition, while the inflow velocity (infiltration) and outflow velocity (exfiltration) calculated from the subsurface flow model is fed back to the surface flow model as the source of water. On the other hand, in the mechanical component, the 3D soil mechanics model based on the linear elastic theory is established by the solid mechanics module in COMSOL to calculate the effective stress and body load. For the slope stability analysis, the local factor of safety (LFS) approach is adopted, enabling the assessment of slope instability across a wide area including multi slopes.

Figure 8 illustrates the entire procedures of the slope stability analysis using the hybrid coupled model. In the analysis, to enhance computational efficiency in large mountainous areas, the 2D shallow water equation is simplified to the diffusion wave equation by omitting some insignificant terms. Consequently, the surface flow is governed by the diffusion wave equation, while the subsurface flow is governed by the 3D Richards equation. The Green-Ampt model is used for calculating the infiltration capacity of the ground surface to determine when runoff occurs. The subsurface flow model in hydraulic component and soil mechanics model in mechanical component are coupled in two ways: (1) the body load function related with the volumetric water content is applied to a linear elastic soil mechanics model to manifest the effect of water content variation on the self-weight and stress distribution; (2) the effect of water content variation on the pore water pressure (matric suction) is considered for evaluating the effective stress and the local factor of safety (LFS) as shown in Equation 1.

$$F_{LFS} = \frac{\tau}{\tau^*} = \frac{2 \cdot \cos\phi'}{\sigma_1' - \sigma_3'}\left[c' + \frac{\sigma_1' + \sigma_3'}{2}\tan\phi'\right] \quad (1a)$$

where, τ : shear strength of soil in current (unsaturated) state (kPa), τ^* : shear strength of soil in saturated state (kPa), c' : effective cohesion (kPa), ϕ' : effective internal friction angle (°), σ_1' and σ_3' : the maximum and minimum principal stress for unsaturated soil based on Bishop's effective stress equation (Bishop, 1954) (kPa).

$$\sigma' = (\sigma - u_a) + \chi(u_a - u_w), \quad \chi = S_e = \frac{S_r - S_{rr}}{S_{rs} - S_{rr}} \quad (1b)$$

where, σ': effective stress (kPa), σ : is total stress (kPa), u_a : pore air pressure (kPa), u_w : pore water pressure (kPa), χ : matric suction coefficient which varies from 0 to 1 depending on the degree of saturation (S_r), S_e, S_{rs} and S_{rr} : effective, saturated and residual degree of saturation.

It is noted that the surface flow model and subsurface flow model is coupled in a bidirectional coupling process, and the subsurface flow model and soil mechanic model is coupled in a unidirectional coupling process. The validity and reliability of the hybrid coupled model and the detailed model building process can be referred at Zhu et al. (2020) and He et al. (2023).

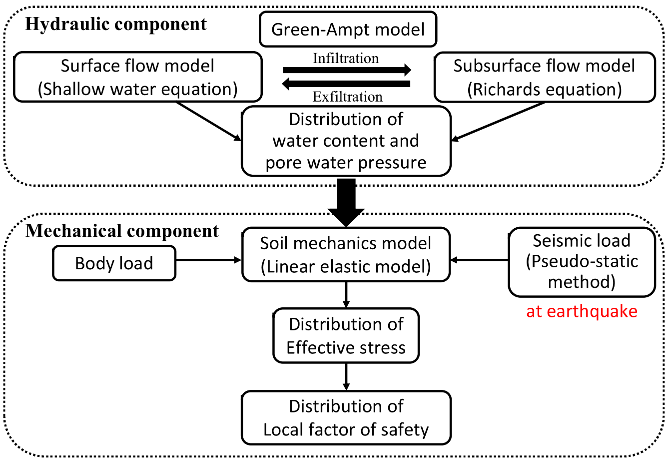

Fig. 8 Analytical procedures for hybrid coupled model with consideration of seismic load.

Pseudo-Static Method in Calculation of Seismic Load

Since the seismic motions cause dynamic forces that can exceed static loads, leading to additional stresses on the soil slope and increasing the potential for collapse, the influence of earthquake should be evaluated for the slope stability analysis (Kawamura et al., 2019). In general, the seismic motions could induce fluctuations in pore water pressure, reducing effective stress of soils like liquefaction and making it more prone to instability and sliding. Besides, the seismic wave may undergo the amplification in specific soil ground or geological formations, intensifying forces on the slope.

Slopes subjected to seismic forces may experience the complex failure mechanisms, necessitating accurate numerical simulation analysis to assess the overall stability. There are two methods to examine the behavior of soil ground and earth structures at earthquake and the effects of seismic motions on the response: (1) Pseudo-static response analysis that converts seismic motions to static forces; (2) Dynamic response analysis that considers seismic motion as an input to the system directly. In Japan, the pseudo-static response analysis is commonly employed for the Level 1 earthquake motion until the JMA seismic intensity of upper 5, while the dynamic response analysis is mainly employed for the Level 2 earthquake motion over the JMA seismic intensity of lower 6. Accordingly, the dynamic response analysis would be recommended for the slope stability analysis under seismic loads for geo-disasters in Shikotsu Lake area on 2018 Hokkaido Eastern Iburi Earthquake as the strong seismic motion with the JMA seismic intensity of lower 6 was observed as shown in Figure 7. However, to enhance the computational efficiency in vast analytical areas, this study employs a little bit larger element size than that in the general dynamic response analysis. For this reason, the pseudo-static response analysis with simpler and faster calculation was adopted as compared with the dynamic response analysis.

The concept of pseudo-static response analysis, which is a method of calculating stability during earthquakes by replacing the effects of earthquake motion with static loads, was first introduced by Mononobe and Okabe (Mononobe, 1929, Okabe, 1924). In the Mononobe-Okabe method, the seismic coefficients in horizontal and vertical directions (K_h, K_v) are used as a coefficient that relates the seismic inertia force (F) acting on a sliding mass or structure to its own weight (W), that is the ratio of acting acceleration (α) to gravitational acceleration (g). The pseudo-static methods have found their ways into various seismic design codes and guidelines around the world. Numerous researchers have contributed to the development and improvement of pseudo-static methods to appropriately estimate the seismic coefficient by comparing the results of pseudo-static methods with those obtained from more sophisticated dynamic response analysis, such as response spectrum analysis and time-history analysis. In this study, the pseudo-static method proposed by Noda et al. (1975) that transforms earthquake waves to a static inertia force (F) with using Equations 2 and 3 was utilized to calculate the stress field at the earthquake event and obtain LFS distribution.

$$F = K_h \text{ or } K_v \cdot W \tag{2}$$

$$K_h, K_v = \frac{\alpha_{max}}{g}, \ \alpha_{max} < 0.2\text{g} \tag{3a}$$

$$K_h, K_v = \frac{1}{3} \cdot \left(\frac{\alpha_{max}}{g}\right)^{\frac{1}{3}}, \ \alpha_{max} > 0.2\text{g} \tag{3b}$$

The entire procedures of the slope stability analysis using the hybrid coupled model when considering seismic actions is also shown in Figure 8. In case of the geo-disasters in Shikotsu Lake area on 2018 Hokkaido Eastern Iburi Earthquake, the maximum ground acceleration (α_{max}) of 559.4 Gal, 384.1 Gal and 325.3 Gal on EW, NS and UD directions recorded at the nearby at the Shikotsu Lake seismic station (HKD185) are converted using Equations 2 and 3 to the seismic coefficients of $K_{h\text{-}EW}$ = 0.276, $K_{h\text{-}NS}$ = 0.244 and $K_{v\text{-}UD}$ = 0.231 respectively, as shown in Figure 9. However, it is reported that this method gives only a conservative seismic inertia force since it is for a rough evaluation of the behavior and response of soil ground and earth structures during an earthquake (Ichii, 2003).

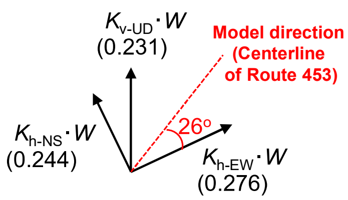

Fig. 9 Acceleration waveforms recorded at 2018 Hokkaido Eastern Iburi Earthquake at Shikotsu Lake seismic station (HKD185).

NUMERICAL SIMULATIONS OF LANDSLIDE DISASTERS

Numerical Simulation for Geo-disasters in Nissho Pass Area

Simulation Model and Analytical Conditions

The slope stability analysis for geo-disasters in the Nissho Pass area is conducted by the hybrid coupled model. A 3D simulation model including two large-scale embankment collapse locations (Location 1 & 2) occurred near the 7th stage of the Nissho Pass area was constructed using the digital elevation model (DEM) based on the 1m laser profile data derived from airborne laser scanning provided by Hokkaido Regional Development Bureau (HRDB) as show in Figure 10a. In addition, to evaluate the influence of the modeling method for the topographic information of the analytical area, another 3D simulation model (Figure 10b) was also constructed using the 10 m DEM provided by Geospatial Information Authority of Japan (GSI). These models are employed in the slope stability analysis under heavy rainfall in order to examine the impacts of various analytical conditions on the interaction between surface and subsurface flows and its effects on the slope instability.

The simulation model is composed of four material parts as shown in Figure 10c: weathered granite, natural soil, embankment, and Asphalt mixture layer (As layer). The natural soil layer and embankment layer were assumed to be 10 m of the layer thickness according to the in-situ investigation, while the thickness of the As layer was set to the common value of 0.35 m. The grid used in the natural soil layer and embankment layer of the 1 m DEM model was 1 m mesh, while for the weathered granite layer, the meshes were set to gradually varied sizes from 1 m to 50 m. It is noted that in case of the 10 m DEM model, the minimum element size was 10 m and the As layer was not modeled. The initial groundwater level was set to −5.5 m from the ground surface according to the historical measured average value in the same period of previous years. For the boundary conditions of the simulation model, in the hydraulic component, the bottom side is the pressure boundary, the lateral side is the no flow boundary, and the surface is the climate boundary combining the rainfall and runoff, as shown in Figure 10c. In the mechanical component, the bottom side is the fixed boundary, the lateral side is the roller boundary, and the surface is the free boundary.

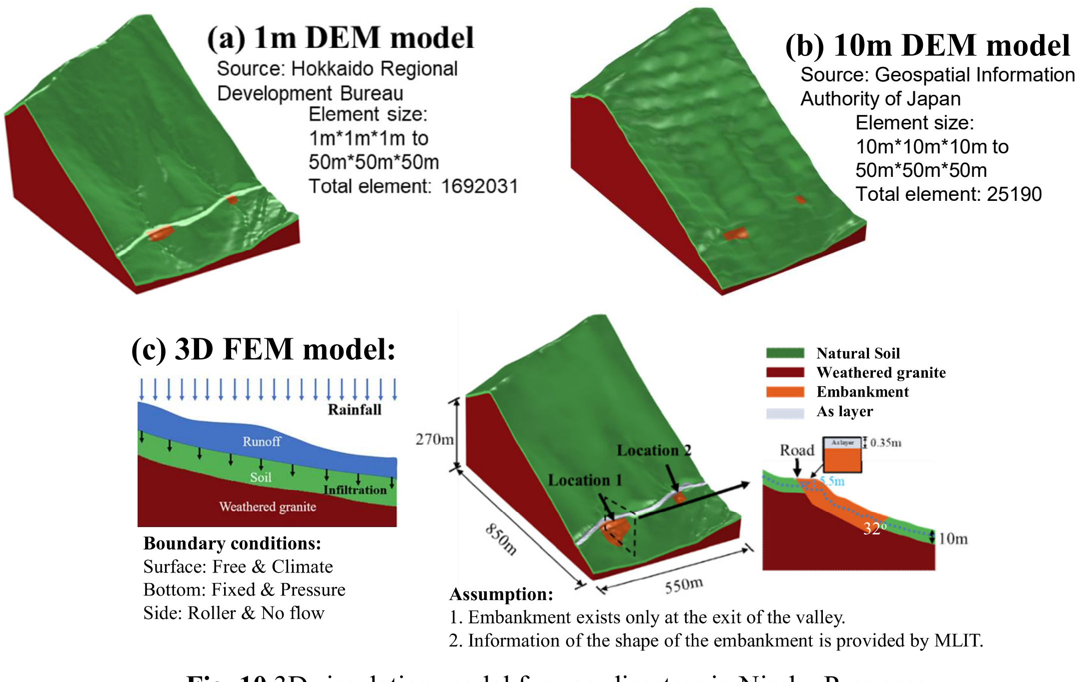

Fig. 10 3D simulation model for geo-disasters in Nissho Pass area.

Among all the input parameters shown in Table 1, for the materials except the As layer, dry density (ρ_d), effective cohesion (c'), effective friction angle (ϕ'), elastic modulus (E), Poisson's ratio (v), saturated hydraulic conductivity (k_s), and saturated volumetric water content (θ_s) were obtained from previous researches (Sato et al., 2017; Zhu et al., 2020; Zhu et al., 2022), while residual volumetric water content (θ_r) and van Genuchten parameters (α and n) were estimated based on the grain size distribution curve of the soil by using the SoilVision software (SoilVision, 2018). For the material of As layer, all the input parameters were determined by referring to the past researches (Nakanishi et al., 2019; Yasuoka et al., 2021). Besides, Manning's roughness coefficient (n_m) was set to 0.300 s/m$^{1/3}$ for the slope (natural soil and embankment), which is the recommended value for mountain grassland by Japan Institute of Country-ology and Engineering (JICE), and 0.100 s/m$^{1/3}$ for the As layer (Chow, 1959), which value is slightly calibrated for easier convergence of the numerical simulation.

Table 1. Material properties used for the simulation of geo-disasters in Nissho Pass area.

Parameters	Embankment	Natural soil	Weathered granite	As layer
Dry density, ρ_d (kg/m^3)	1695.0	1020.0	2000.0	2400.0
Effective cohesion, c' (kPa)	0	0	37.0	82.0
Effective friction angle, ϕ (°)	37.0	35.0	21.0	41.0
Elastic modulus, E (MPa)	10.0	15.0	500.0	3000.0
Poisson's ratio, v	0.30	0.30	0.30	0.35
Saturated hydraulic conductivity, k_s (m/s)	1.12×10^{-5}	1.40×10^{-6}	3.47×10^{-9}	1.00×10^{-8}
Saturated volumetric water content, θ_s (m^3/m^3)	0.360	0.630	0.480	0.070
Residual volumetric water content, θ_r (m^3/m^3)	0.035	0.190	0.008	0.014
van Genuchten parameter, α (m^3/m^3)	0.538	0.810	0.012	22.830
van Genuchten parameter, n	0.468	0.437	0.246	1.940
Manning's roughness coefficient, n_m (s/m$^{1/3}$)	0.300	0.300	–	0.100

Analytical Procedures of Slope Stability Analysis

The analytical procedures of slope stability analysis could be summarized into several steps as follows: (1) "Initial stress analysis" by self-weight and initial groundwater level to obtain the initial distribution of effective stress and pore water pressure in the initial equilibrium of the model. (2) "Transient response analysis" using the hydraulic component under the rainfall history shown in Figure 3. The coupled surface and subsurface flow analysis was conducted under rainfall boundary condition. (3) "Slope stability analysis" under heavy rainfall using the mechanical component, taking into account the simulation results obtained from the transient response analysis due to rainfall. Based on the distribution of water content and pore water pressure from the transient response analysis, the distribution of the local factor of safety (LFS) at each time step was calculated by recalculation of stress field in the initial equilibrium. The simulation time is from 19:00 on August 28th, 2016 to 17:00 on August 31st, 2016 for a total of 70 hours with the timestep of 1 hour. For comparison, a slope stability analysis under heavy rainfall was also conducted separately based on the simulation results obtained from the transient response analysis due to rainfall without considering surface flow.

Numerical Simulation for Geo-disasters in Shikotsu Lake Area

Simulation Model and Analytical Conditions

The slope stability analysis for geo-disasters in the Shikotsu Lake area (Case 1 and Case 2) is conducted by the hybrid coupled model. However, in case of considering the seismic motions (Case 2), it would incorporate the seismic loads into numerical simulations by the pseudo-static method as shown in Figure 8. Figure 11 shows two 3D simulation models of targeted mountainous areas, which were constructed using 1 m laser profile data provided from the HRDB. These models are employed for both slope stability analysis under heavy rainfall and slope stability analysis under seismic motion after heavy rainfall, with focusing on the influences of coupled surface and subsurface flow. The geometry of the simulation model is composed of two layers as shown in Figure 11: the topsoil layer which is assumed to be 4 m of the layer thickness according to the in-situ investigation, and the bedrock layer which is the rest area of the model. However, it is noted that the bedrock is strongly weathered shale. The grid used in the topsoil layer of the two models was 1 m mesh, while for the bedrock layer, the meshes were set to gradually varied sizes from 1 m to 20 m. The initial ground water level was set to −2.45 m below the surface for both models according to the historical measured average value. Figure 11 shows the boundary conditions of the simulation model for the hydraulic and mechanical components. Among all the input parameters shown in Table 2, dry density (ρ_d), effective cohesion (c'), effective friction angle (ϕ'), elastic modulus (E), and Poisson's ratio (v) were determined by referring to the disaster investigation report with HRDB. For the rest hydraulic input parameters (k_s, θ_s, θ_r, α, and n) with lack of data, they were assumed to be the same values used in numerical simulations for the Nissho Pass area as the soil types are similar.

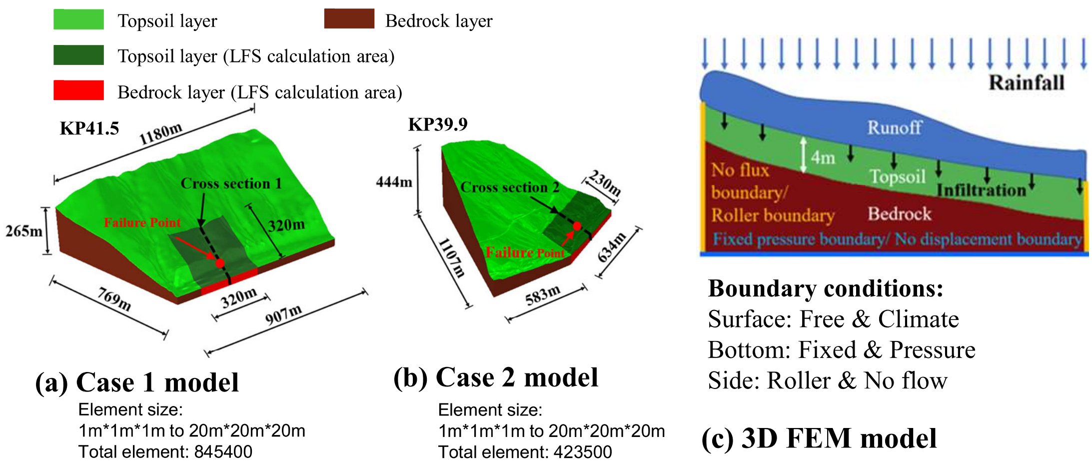

Fig. 11 3D simulation model for geo-disasters in Shikotsu Lake area.

Table 2. Material properties used for the simulation of geo-disasters in Shikotsu Lake area.

Parameters	Topsoil (Case 1)	Topsoil (Case 2)	Bedrock (Case 1)	Bedrock (Case 2)
Dry density, ρ_d (kg/m^3)	641.0	531.0	735.0	735.0
Effective cohesion, c' (kPa)	0	1.0	1.0	1.0
Effective friction angle, ϕ (^{o})	30.0	24.0	31.0	31.0
Elastic modulus, E (MPa)	2.1	7.0	31	31
Poisson's ratio, v	0.3	0.3	0.3	0.35
Saturated hydraulic conductivity, k_s (m/s)	2.0×10^{-6}	1.40×10^{-6}	3.47×10^{-9}	3.47×10^{-9}
Saturated volumetric water content, θ_s (m^3/m^3)	0.630	0.630	0.480	0.480
Residual volumetric water content, θ_r (m^3/m^3)	0.190	0.190	0.008	0.008
van Genuchten parameter, α (m^3/m^3)	0.810	0.810	0.012	0.012
van Genuchten parameter, n	1.776	1.776	1.326	1.326
Manning's roughness coefficient, n_m (s/m$^{1/3}$)	0.300	0.300	–	–

Analytical Procedures of Slope Stability Analysis

The analytical procedures of slope stability analysis could be summarized into several steps as follows: (1) "Initial stress analysis" by self-weight and initial groundwater level. (2) "Transient response analysis" using the hydraulic component under the rainfall history shown in Figure 6. (3) "Slope stability analysis" under heavy rainfall using the mechanical component, taking into account the simulation results obtained from the transient response analysis due to rainfall. (4) "Slope stability analysis" under seismic loads using the mechanical component, taking into account the simulation results obtained from the transient response analysis due to rainfall. Based on the distribution of water content and pore water pressure from the transient response analysis, the distribution of the LFS at the earthquake occurrence time (03:07am on September 6th, 2018) was calculated by statically applying the seismic accelerations shown in Figure 9 in accordance with the pseudo-static method using Equations 2 and 3. The simulation time for Case 1 and Case 2 is from 08:00 on September 3rd, 2018 to 03:00 on September 6th, 2018 for a total of 67 hours with the timestep of 1 hour. For comparison, a slope stability analysis under seismic loads in the absence of preceding rainfall was also conducted separately. It is noted that due to the low convergence speed of the large model, this study employed a smaller area for the LFS calculation in the mechanical component, which is shown in the dark green square box of Figure 11. However, this approach would not significantly impair the precision in the LFS calculation since the local effective stress remains unaffected by the variation in the calculation area.

SIMULATION RESULTS AND DISCUSSIONS

Numerical Simulation for Geo-disasters in Hidaka Mountains Area

Influence of Runoff on Slope Stability

In order to investigate the influence of runoff on the slope stability, two simulation results derived from slope stability analyses with and without considering runoff are compared. Figure 12 shows the distribution of local factor of safety (F_{LFS}) at the elapsed time (t) of 54 hours when the hourly rainfall reaches its maximum value (at 01:00 on August 31st, 2016 in Figure 3) in the two cases. This clearly identifies the difference between stable and unstable parts during heavy rainfall. With considering runoff (Figure 12b), the unstable area of 100 m wide and 50 m long is spread in Location 1, while the unstable area of 40 m wide and 40 m long is spread in Location 2. Conversely, without considering runoff (Figure 12a), the unstable area is very small as compared with Figure 12b, and the slope failure only occurred in a very narrow part at both locations. In addition, Figure 13 shows the distribution of pore water pressure (u_{w}) and F_{LFS} at the cross section situated at the black dash line in Figure 10c. With considering runoff, it causes a significant increase in pore water pressure from negative value to positive value in the surface layer of the embankment, which results in the slope instability. The unstable area extends to a deep part of the embankment reaching 3m at Location 1. On the contrary, without considering runoff, the increment of the pore water pressure is hardly observed. As a result, the failure depth is much smaller than the case with considering runoff, and the shallow slope failure is very shallow and negligible at both Location 1 and Location 2. These indicate that by considering runoff occurred in the real during heavy rainfall, the slope stability analysis using the hybrid coupled model can appropriately reproduce the situations of actual slope failures. However, compared with the failure scale in situ (blue dash line in Figure 13b) reported in the disaster investigation report (JGS, 2017), even when considering runoff, the real slip surface at Location 1 is extremely deeper than the simulation results, though the simulation results can well reproduce that at Location 2. This underestimation of the slip surface depth at Location 1 is considered due to the results of ignoring in this study the erosion effect caused by high-speed runoff water with large amount that can wash away the surface soil particle to expose underearth layer.

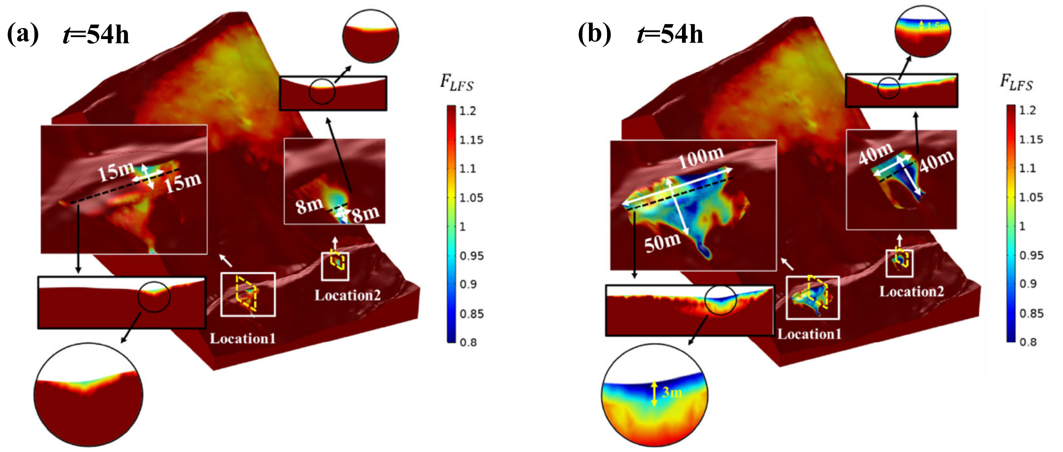

Fig. 12 Distribution map of F_{LFS} at the 7th stage in Nissho Pass: (a) Without considering runoff; (b) With considering runoff (after He et al. 2023).

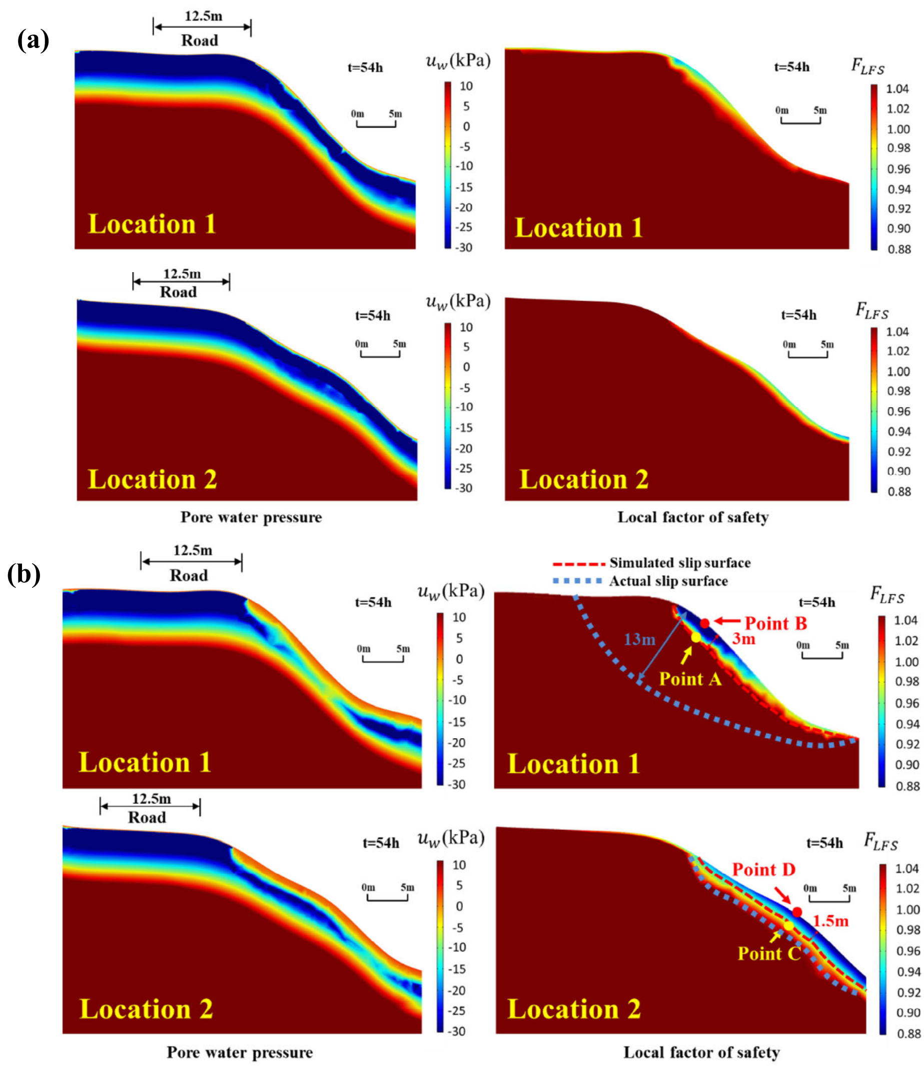

Fig. 13 Distribution map of F_{LFS} and u_{w} at the cross section of two locations in Nissho Pass area: (a) Without considering runoff; (b) With considering runoff (after He et al. 2023).

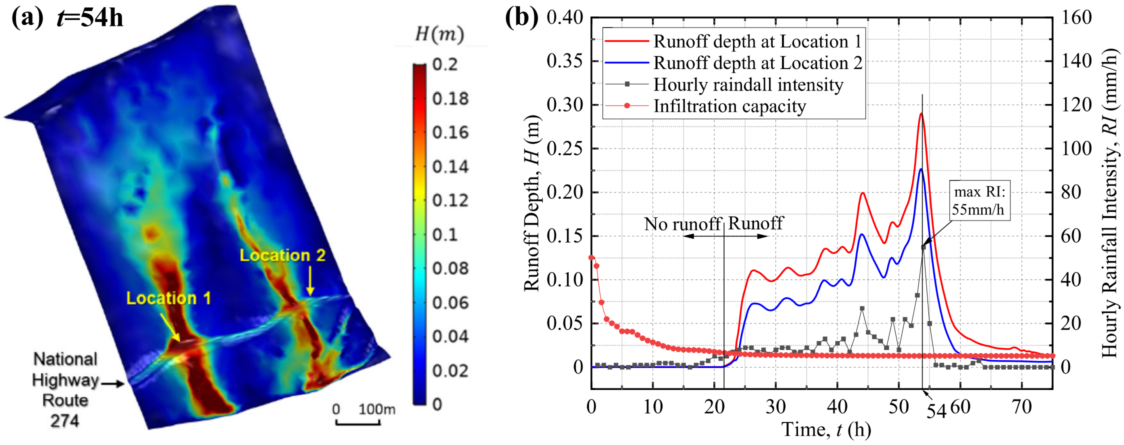

Fig. 14 Simulation results with considering runoff: (a) Distribution map of runoff depth at the 7th stage in Nissho Pass (after He et al. 2023); (b) Change in runoff depth with time.

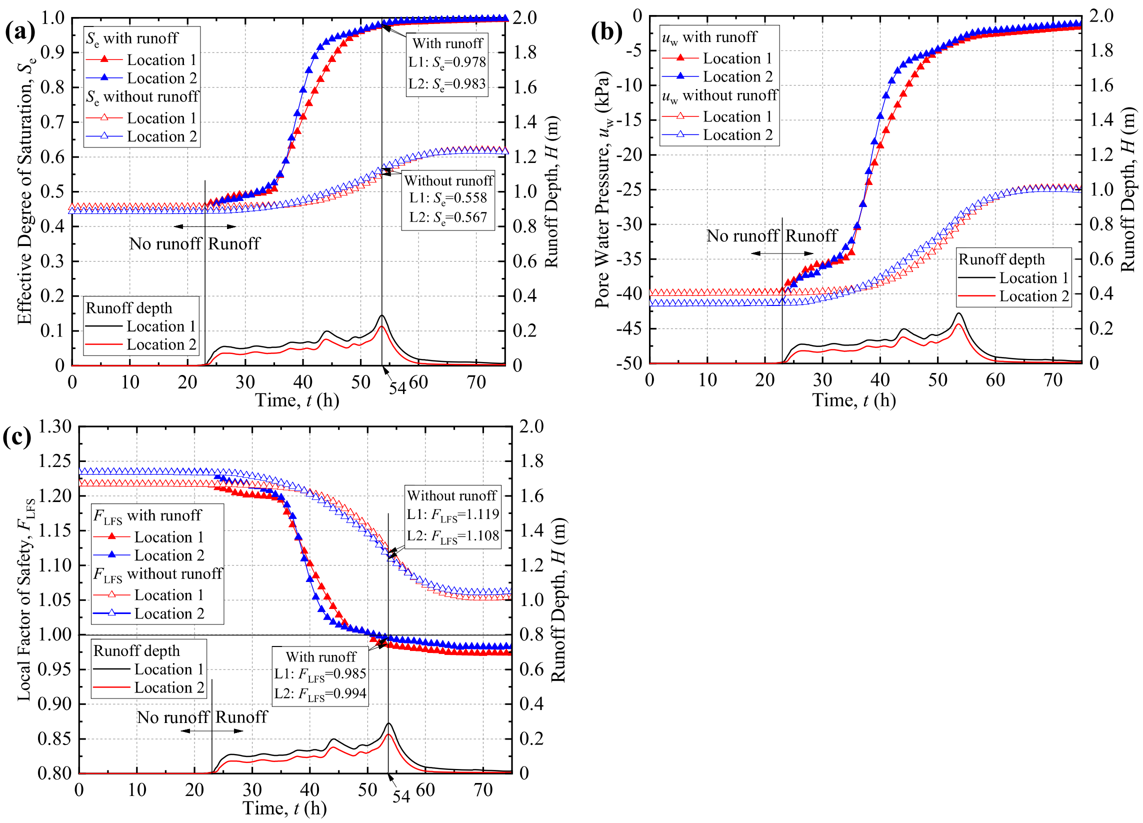

Fig. 15 Change in simulation results with time: (a) Effective degree of saturation (S_e); (b) Pore water pressure (u_w); (c) Local factor of safety (F_{LFS}).

Figure 14a plots the distribution of runoff depth calculated in the hydraulic component at t = 54 hours. It can be seen that a large amount of surface water from the upstream catchment and road is gathered at both locations, especially Location 1, allowing more water to infiltrate into the embankment, which is the exact point of embankment collapse. On the other hand, Figure 14b shows the change in runoff depth with time at both locations, and the hourly rainfall intensity along with the infiltration capacity. With continuous rainfall, the infiltration capacity of the soil ground dramatically decreases, and around the 22nd hour, the rainfall intensity exceeds the infiltration capacity, which is the time that runoff generates along the slope surface. In this case, the trend of the runoff depth at both locations fits with the trend of rainfall intensity, meaning that heavy rainfall will provide enough water to form the surface runoff in the catchment area. Besides, Figure 15 shows the change in effective degree of saturation (S_e), pore water pressure (u_w), and local factor of safety (F_{LFS}) with time at Location 1 and Location 2 (Point A and Point C in Figure 13b, located near the slip surface of numerical simulations). The infiltrated water causes the increase of the degree of saturation, which causes an increase of the pore water pressure, thereby causing a decrease in the shear strength of unsaturated soils, and finally decreases the F_{LFS}. In addition, the increase of S_e and u_w, and the decrease of F_{LFS} are more significant with considering the runoff. After the runoff generation, S_e and u_w dramatically increase and F_{LFS} sharply declines, meaning that the runoff from upstream allows more water to infiltrate into the embankment and more significant decrease in the shear strength of the embankment. These indicate that the possibility of embankment collapse at the runoff cumulated point such as the exit of the gully becomes higher than other locations along the highway, and that the runoff is a key factor, which cannot be ignored, to be considered in the wide-area slope stability analysis during extremely heavy rainfall.

Influence of Modeling Method for Topographic Information on Slope Stability

In order to examine the influence of modeling method for topographic information on the slope stability, two simulation results derived from slope stability analyses using 1 m and 10 m DEM models with considering runoff are compared. Figure 16 shows the change in runoff depth with time. With continuous raining, the infiltration capacity decreases, thereby generating runoff at 20 hours from the beginning of the simulation. Both 1 m and 10 m DEM models are able to reproduce the phenomenon of water accumulation at two embankment collapse locations. However, there exist several differences in the detailed simulation results between these two models. The simulated depth of slip surface at Location 1 for 1 m DEM model is distinctly higher than that for 10 m DEM model, while at Location 2 there seems no great difference between the results. It can be attributed to a cause that the surface flow along the road from Location 2 to Location 1 since 1 m DEM model can reproduce since 1 m DEM model traces the 3D shape of road precisely while 10 m DEM model cannot realize it (Figure 17). As shown in Figure 10, 10 m DEM model is too coarse to reproduce the road shape correctly as compared to 1 m DEM model because the general width of a road is about 3.5m on each side. Hence, by the impact of the surface flow which cannot be simulated in 10 m DEM model, the runoff depth at Location 1 in 1 m DEM model is higher than that in 10 m DEM model, and approaches to the realistic situation.

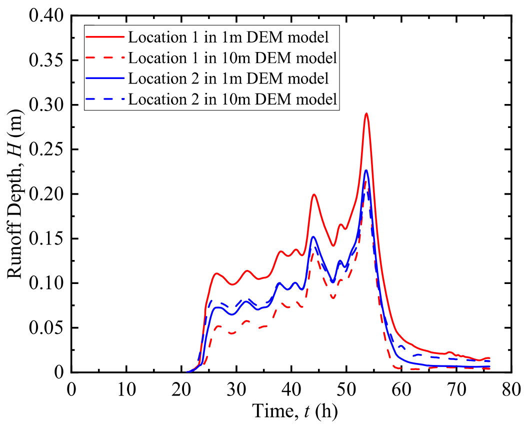

Fig. 16 Influence of modeling method on change in runoff depth with time.

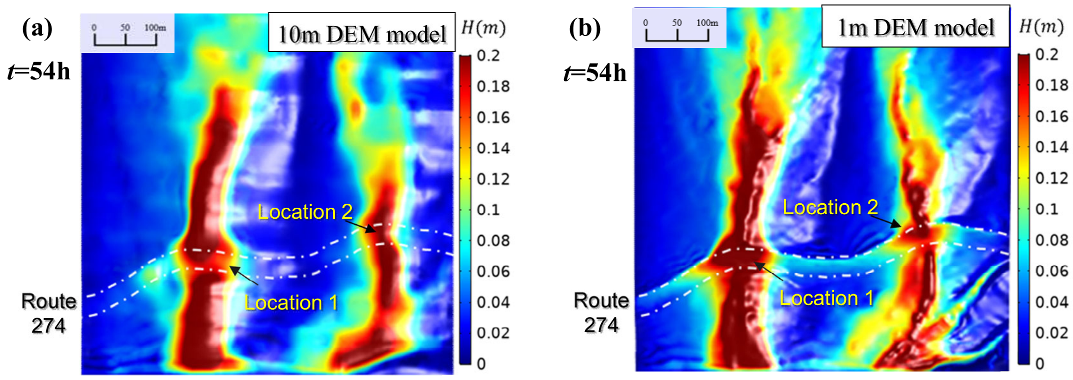

Fig. 17 Distribution map of runoff depth at the 7th stage in Nissho Pass: (a) 10 m DEM model; (b) 1 m DEM model.

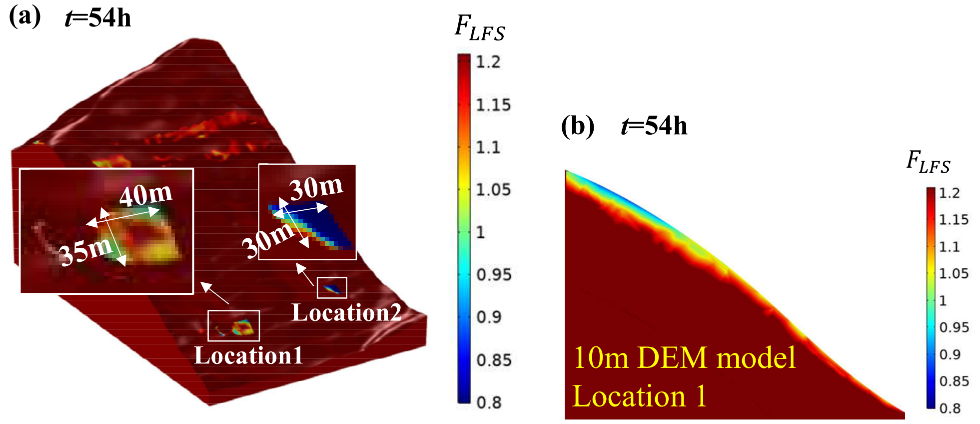

Fig. 18 Distribution map of runoff depth at the 7th stage in Nissho Pass: (a) 10 m DEM model; (b) the cross section of Locations 1.

Figure 18 shows the distribution of local factor of safety (F_{LFS}) at the elapsed time (t) of 54 hours in the 10 m DEM model with considering runoff. Comparing Figure 18 with Figure 12, the unstable area (blue color area) at Location 1 in 10m DEM model is clearly smaller than that in 1m DEM model, and the slip surface is hardly confirmed. This is because of the higher runoff depth in the latter model. High depth runoff increases the water pressure at the surface boundary resulting more water infiltrating into the soil ground to degrade the slope stability. Furthermore, compared with the failure scale in situ reported in the disaster investigation report (JGS, 2017), 1 m DEM model can reproduce the situations of actual slope failures well at both locations, while the unstable area at Location 1 in 10m DEM model is considerably smaller than the case in situ. By using DEM data with high precision, analysis can reproduce the flow of surface water along roads during heavy rainfall, which indicates that utility of using high-precision DEM data in wide-area landslide risk assessment is indispensable. Therefore, the slope stability analysis considering rainfall infiltration and runoff can simulate the flow of surface water along roads during heavy rainfall accurately by using detailed DEM model, thus leading to the importance of the usage of high-precision DEM data in a wide-area risk assessment of slope instability under climate change.

Influence of Asphalt Layer on Slope Stability

In practice, the impervious covering system on the slope such as the concrete spraying method reduces the rainwater that infiltrates into the soil ground, leading to the prevention and mitigation of geo-disasters. Accordingly, the impervious asphalt (As) layer of roads and pavements is considered to effectively prevent the runoff-induced slope failure in the same manner as shotcrete. In this section, to examine the influence of As layer on the runoff and slope stability, the simulation results obtained from two case studies, that is "with and without considering As layer" on the road surface, are compared. Here, in case of "without As layer", the input parameters of As layer in Table 1 were replaced by those of the material beneath it (embankment or natural soil).

Figure 19 compares the distribution of runoff velocity in the two cases. With considering As layer, the runoff velocity along the road at Location 1 and 2 becomes much higher than that without considering As layer, and consequently, high-speed runoff exceeding the critical erosion velocity causes the erosional damage of pavement and embankment in the wide area. Figure 20 shows the change in runoff depth and runoff velocity on the road (Point E and Point F in Figure 19, located on the road center) with time. With considering As layer, the runoff along the road generates earlier due to the low permeability of As layer. In addition, the difference between maximum runoff depth of two cases is not very large, while the maximum runoff velocity with considering As layer is higher than that without considering As layer because of the low surface roughness of As layer. This means that the As layer accelerates the runoff velocity and causes more surface water flow along the road to impact the embankment on the roadside during heavy rainfall.

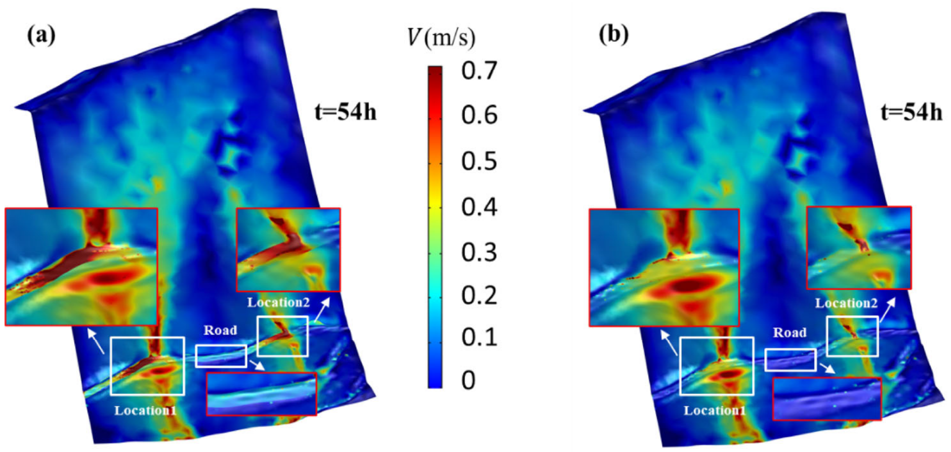

Fig. 19 Distribution map of runoff velocity at the 7th stage in Nissho Pass: (a) With considering As layer; (b) Without considering As layer (after He et al. 2023).

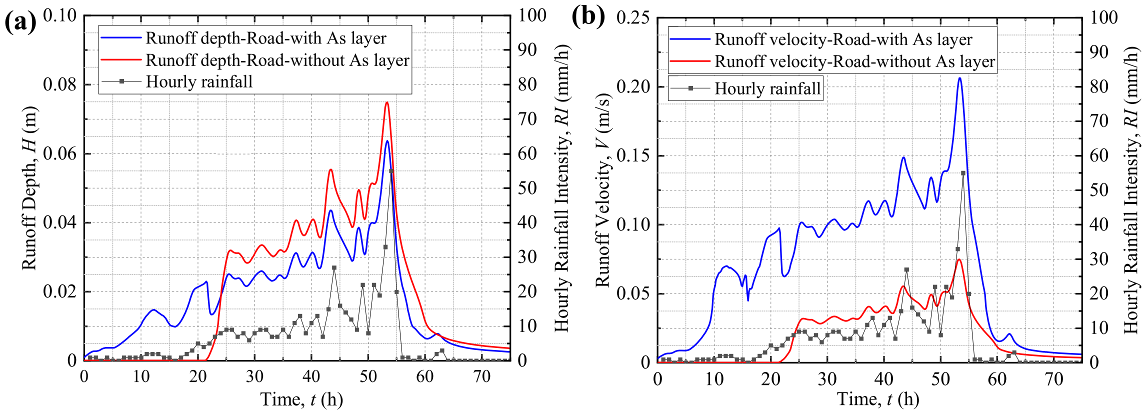

Fig. 20 Influence of As layer on change in simulation results with time: (a) Runoff depth; (b) Runoff velocity.

On the other hand, the low permeability of asphalt layer prevents more water to infiltrate into soil ground and embankment, which can enhance the slope stability and reduce the risk of geo-disasters. Figure 21 shows the distribution of pore water pressure (u_w) and local factor of safety (F_{LFS}) at both locations in case of without considering As layer. As layer keeps low pore water pressure in the embankment, while without considering As layer, a large amount of water infiltrates from the road surface. Comparing Figure 21 with Figure 13b, the local factor of safety around the road in case of with considering As layer is larger than the case without considering As layer, meaning that the As layer with low permeability can keep the slope stability and reduce the failure scale around the road (green dashed box in Figure 21). Especially at Location 2, the actual slope failure occurs at only roadside embankment. This pattern of slope failure agrees well with the simulation results with considering As layer. As for the above-mentioned underestimation of the slip surface depth at Location 1, it is considered that damages in the As layer caused by the initial slope failure accelerated the infiltration and erosion, leading to more serious failure including the road part. These indicate that the material properties such as infiltration capacity and surface roughness etc. of As layer seriously affect the runoff flow and slope stability during heavy rainfall, and suggest that an appropriate combination for the material properties of pavement structures has a potential to significantly contribute to the disaster prevention/mitigation measures of transportation infrastructures.

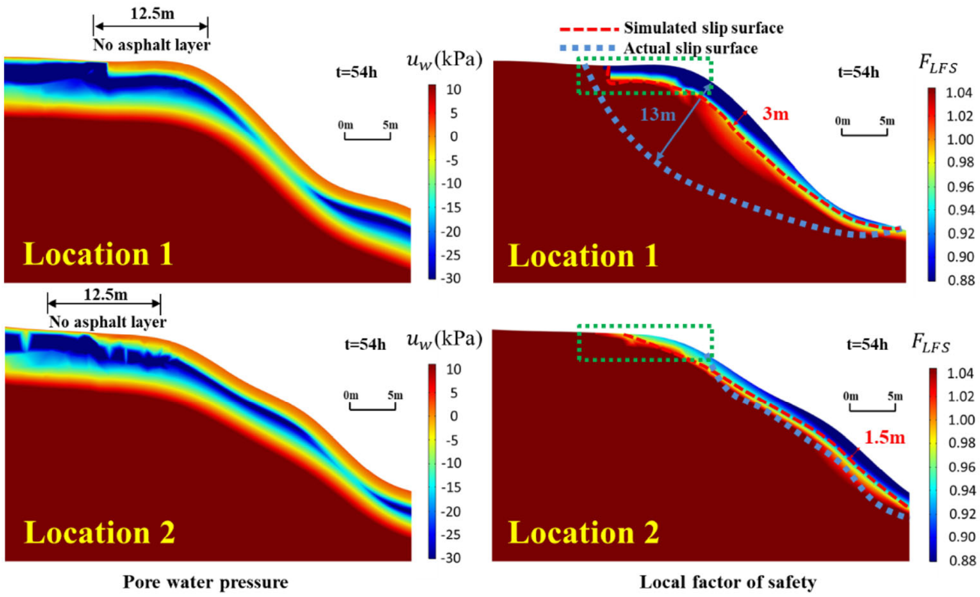

Fig. 21 Distribution map of F_{LFS} and u_{w} at the cross section of two locations in Nissho Pass area without considering As layer (after He et al. 2023).

Numerical Simulation for Geo-disasters in Shikotsu Lake Area

Influence of Topography on Slope Stability

In order to examine the influence of topographic factors on the slope stability, two simulation results derived from slope stability analyses with considering runoff conducted for two slope failure cases occurred in adjacent catchment basins are compared. Figure 22 shows the distribution of runoff depth at two slope failure sites (Case 1 and Case 2) calculated in the hydraulic component at the elapsed time (*t*) of 42 hours when the hourly rainfall reaches its maximum value (at 02:00 on September 5th, 2018 in Figure 6). In Case 1, a tendency for surface flow to accumulate around the slope failure site can be confirmed, while in Case 2, although the runoff water is confirmed surrounding the slope failure site, the inflow into the slope failure site is hardly observed. One reason for this difference in the flow of surface water between two cases is considered to be that the topography of Case 1 like a valley terrain is slightly easier to collect rainwater and surface water from the surrounding area than other areas. On the other hand, in case of Case 2, there is a possibility that the influx of the surface water to the slope failure site was blocked by the existence of a national highway located above the slope failure site, which behaves as an outflow path of surface flow. The variations of runoff depth and infiltration capacity with time are shown in Figure 23. Compared with Case 2 where the runoff generation is hardly seen even if the rainfall intensity exceeds the infiltration capacity of the soil ground, the runoff depth in Case 1 sharply increases in accordance with the increment of rainfall intensity, and it reached the highest value of around 0.3 m at the maximum rainfall intensity (t = 42 hours). From these simulation results, it could be concluded that the heavy rainfall played a more significant role on the runoff generation in Case 1 than Case 2 due to the difference in the topography between the two simulation areas.

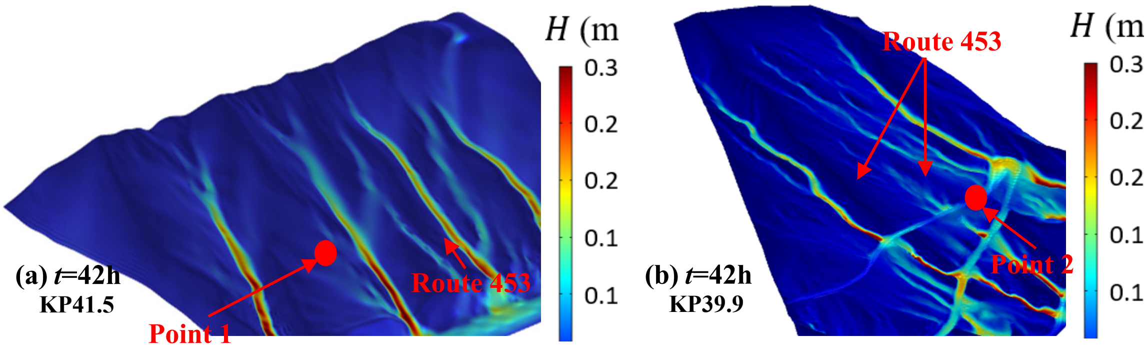

Fig. 22 Distribution map of runoff depth at two slope failure sites in Shikotsu Lake area: (a) Case 1 (KP41.5); (b) Case 2 (KP39.9).

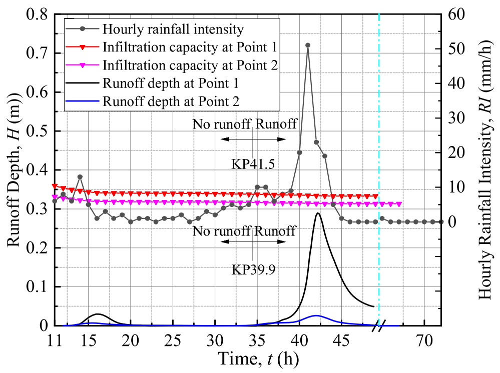

Fig. 23 Change in runoff depth and infiltration capacity with time at two slope failure sites in Shikotsu Lake area.

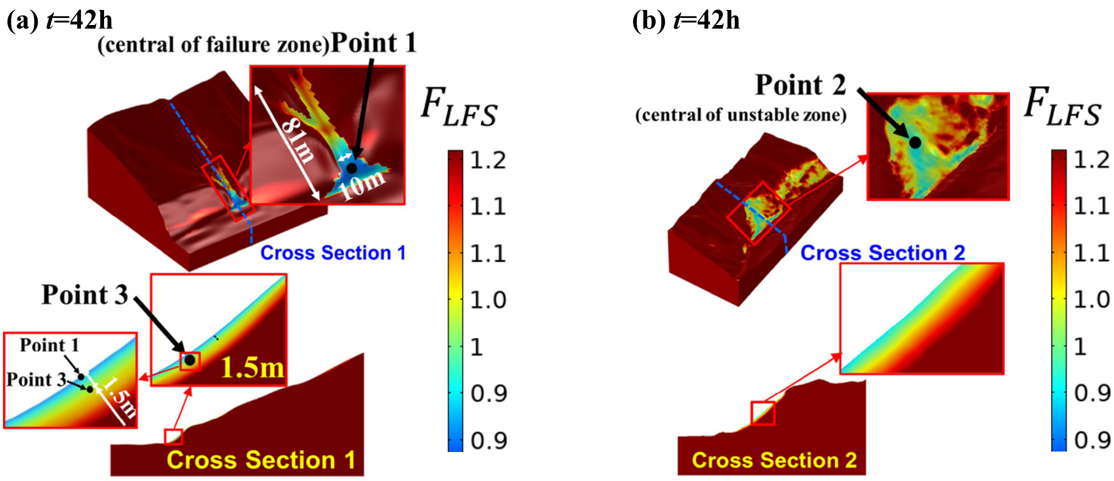

Fig. 24 Distribution map of F_{LFS} at two slope failure sites in Shikotsu Lake area at the maximum rainfall intensity: (a) Case 1 (KP41.5); (b) Case 2 (KP39.9).

Figure 24 shows the distribution of local factor of safety (F_{LFS}) at t = 42 hours derived from slope stability analyses with considering runoff in Case 1 and Case 2. In Case 1, an unstable part with a very low F_{LFS} is distributed in a narrow range (10 m wide, 80 m long, 1.5 m thick in Figure 24a) along the water catchment topography including the slope failure site. The exit of the gully valley, especially the area near the road where slope angle is steep, was calculated to be the most vulnerable zone in the simulation area. Compared with the failure scale in situ reported in the disaster investigation report with HRDB, the simulation results can reproduce the situations of actual slope failures well, thus indicating the applicability of the proposed the slope stability analysis using the hybrid coupled model to the practical use. On the other hand, though the unstable part in Case 2 is widely distributed around the slope failure site in comparison with Case 1, the local factor of safety is higher than in Case 1, and the risk of slope failures is lower like the real case. In other words, the differences in the surrounding topography greatly affected the catchment ability of rainwater and surface water near the slope failure site. According to the disaster investigation report with HRDB, the slope angle and the soil composition of the slip surface are considered to be similar for both slope failure sites. Therefore, the cause of slope failure is considered to be the difference mainly in the topographical and stratigraphical factors, which seriously govern the catchment ability and infiltration capacity at the collapsed sites. In Case 2 with wider unstable part than Case 1 as shown in Figure 24, the infiltration of rainwater and surface water into the soil ground was dispersed, and the rate of increase in water content was correspondingly slowed down as compared to Case 1. As a result, it can be concluded that the cut slope in Case 2 would not have led to collapse by rainfall water alone. This case study also suggests the significance in conducting a 3D slope stability analysis during heavy rainfall using wide-area detail topographic information.

Influences of Earthquake and Preceding Rainfall on Slope Stability

From the discussion in the former section, it was revealed that due to the difference in the topography and stratigraphy of the slope failure sites, Case 1 with high catchment ability collapsed due to heavy rainfall, while Case 2 would not have led to collapse by the rainfall alone. To confirm the validity of this consideration, this section evaluates the influences of earthquake and preceding rainfall on the slope stability. Figure 25 shows the change in runoff depth and local factor of safety (F_{LFS}) with time at Points 1 to 4 in Case 1 and Case 2 (Points 1 and 2 on the ground surface at the central of unstable parts, and Points 3 and 4 near the slip surface of numerical simulations show in Figure 24). Besides, Figure 26 shows the distribution of local factor of safety (F_{LFS}) just before and after the earthquake (at 03:07 on September 6th, 2018, t = 67 hours after rainfall began) derived from slope stability analyses with considering runoff in Case 2. In Case 1, the F_{LFS} value heavily goes down when the runoff takes place. The reason can be understood by referring to the variation of pore water pressure as discussed above. For example, when the runoff depth gets higher, the water pressure at the surface boundary would be increased, which leads to more infiltration into subsurface and causes a higher pore water pressure, thus resulting in the degradation of slope stability. The variation of the F_{LFS} value in Case 2 shows a similar trend with Case 1, while in a smaller magnitude during runoff occurrence period. This can be attributed to little change in pore water pressure caused by very shallow runoff depth in comparison to Case 1. As a result, there is no significant difference of F_{LFS} distribution between the time showing the maximum rainfall intensity (t = 42 hours) and the moment just before the earthquake (t = 67 hours) as shown in Figure 26. Therefore, no slope failure has occurred at the moment just before the earthquake, which is consistent with the actual phenomenon.

However, after the earthquake, the F_{LFS} value in Case 2 sharply declined due to highly varied stress field by strong seismic motion, and the slope failure was incurred. In Figure 26b, an unstable part with a low F_{LFS} is distributed in a wide range (41 m wide, 79 m long, 2.1 m thick). These simulation results are consistent with the fact that the slope failure in Case 2 was discovered after the earthquake, and the range of the unstable part also matches almost the scale of the actual slope failure. Furthermore, Figure 27 shows the distribution of F_{LFS} just before and after the earthquake derived from slope stability analyses without considering preceding rainfall (Figure 6) before the earthquake in Case 2. Comparing Figure 27 with Figure 26, the unstable part (blue color part) is hardly seen even after the earthquake in case of without considering preceding rainfall, and the slip surface is not clearly confirmed, meaning that Case 2 would not have led to collapse by the earthquake alone. This suggests that the slope failure observed at Case 2 may have been a compound geo-disaster by heavy rainfall and severe earthquake. From these discussions, it could be concluded that the slope stability analysis using the hybrid coupled model incorporating the pseudo-static method of seismic loads proposed in this study can appropriately evaluate the impact of seismic motion on the stress field change as well as the effect of complex interaction on the pore water pressure variation between runoff and infiltration, and it has a sufficient reproducibility when simulating the earthquake/rainfall induced slope failure.

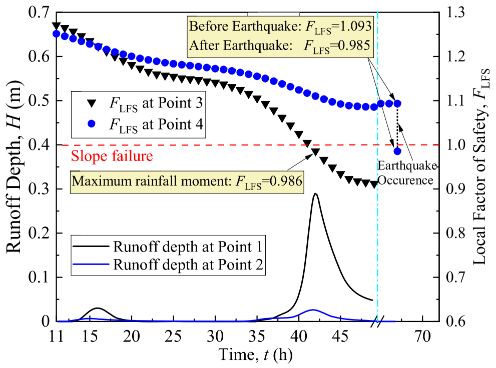

Fig. 25 Change in runoff depth and local factor of safety (F_{LFS}) with time at two slope failure sites in Shikotsu Lake area.

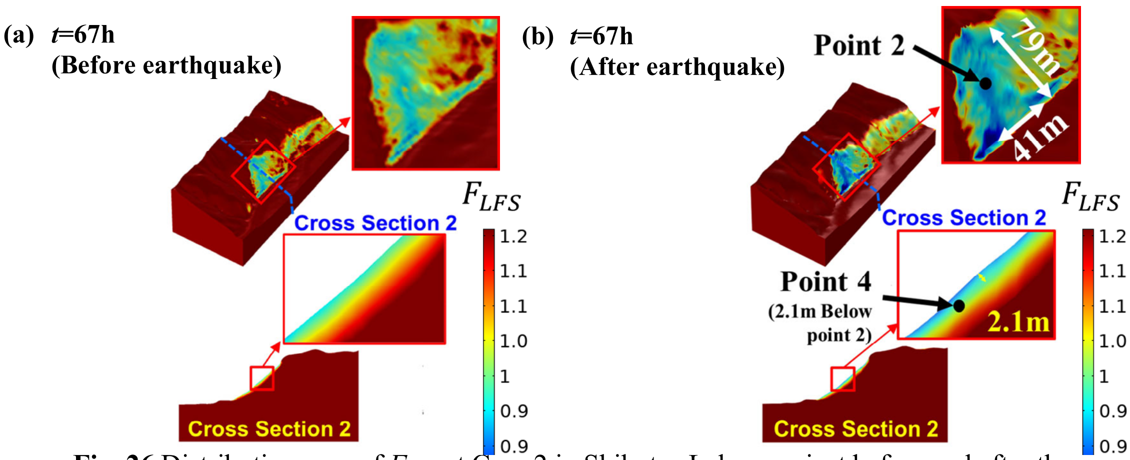

Fig. 26 Distribution map of F_{LFS} at Case 2 in Shikotsu Lake area just before and after the earthquake: (a) Before earthquake; (b) After earthquake.

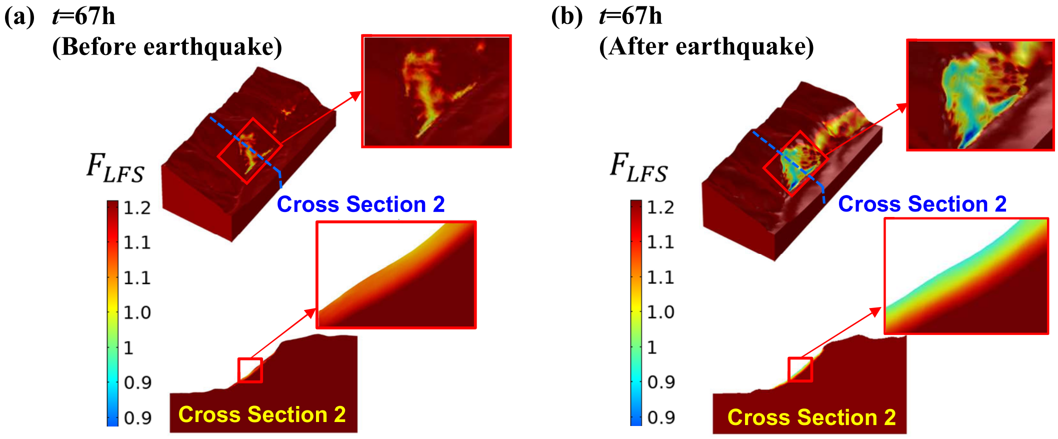

Fig. 27 Distribution map of F_{LFS} at Case 2 in Shikotsu Lake area just before and after the earthquake without considering preceding rainfall: (a) Before earthquake; (b) After earthquake.

Role of Road Network toward Geo-disaster Prevention and Mitigation

This section discusses the perspectives necessary for the risk assessment of transportation infrastructures as a linear structure such as road pavement and examines the role of road network toward the geo-disaster prevention and mitigation under the climate change, based on the simulation results in this study. From case studies of the actual geo-disasters conducted in this study, the following findings for the risk assessment of transportation infrastructures and the geo-disaster countermeasures are mainly obtained:

- During heavy rainfall, runoff generates depending on the infiltration capacity of soil ground, and runoff water flows on the paved surface along the road. Runoff generation accelerates the infiltration of rainwater and surface water into soil ground, thus inducing the quick degradation of slope stability.
- At the case study (Case 2) of Shikotsu Lake area, the road network plays a role in resisting runoff-induced geo-disasters by refraining the inflow of surface water, and conversely, at the case study (Location 1) of Nissho Pass area, the road network acts as a driving force for the geo-disasters by becoming an outflow path of surface flow.
- In case, the road structures with low surface roughness such as As layer induces the increase in runoff velocity to accelerate the surface erosion of soil ground along the road, while in another case, the impermeability of As layer prevents the infiltration of rainwater and surface water into soil ground. In practice, similar measures are often applied in various slope protection methods.
- When the pavement structure is damaged due to erosion of the pavement surface by runoff and debris flow, or cracks in the pavement surface due to embankment collapse, the flow of rainwater and surface water into soil ground would increase, thereby expanding the collapse scale of the slope.
- There is a possibility that the risk of compound geo-disasters would increase as extreme weather events occur more frequently due to the climate change in the future. In this case, if two triggered factors like rainfall and earthquake act in synergy, a geo-disaster may occur under conditions that would not normally occur. Accordingly, it is important to prepare for compound geo-disasters.

Among these findings, some indicate that appropriate selections and combinations of the influencing factors which seriously affects the flow of surface water (e.g. topography of catchment basin, infiltration capacity of soil ground, road alignment, shape/structure/material of pavement) are important for developing the rational countermeasures against runoff-induced slope failures, also suggesting a possibility of planning comprehensive disaster prevention and mitigation measures in terms of the design and construction for transportation infrastructures. For example, if the alignment of road network and the shape of road structures could be changed according to the catchment topography, it would be possible to suppress slope failures caused by the accumulation of surface water flows, as seen at the outflow path. In fact, at other slope failure sites in the Nissho Pass area, geo-disaster examples were confirmed where median strips of the road controlled the flow of surface water and debris flow, causing slope disasters to occur in an unexpected location at the flow end where the median strip is not installed as shown in Figure 28. Moreover, this study revealed that the material properties such as infiltration capacity and surface roughness etc. of As layer seriously affects the runoff flow and slope stability during heavy rainfall. This suggests that when the designer of road networks appropriately selects the surface roughness of road pavement and/or the permeability of pavement structures by considering the flow path network of surface water under heavy rainfall, the risk of runoff-induced slope failures can be mitigated even if the rainfall intensity exceeds the infiltration capacity of soil ground. In this case, the permeable pavement and drainage pavement may show a potential to greatly contribute to the disaster prevention/mitigation measures of transportation infrastructures (Babu et al., 2019). Furthermore, by considering the design of earth structures along road pavement together with the design of pavement structures after examining the high accumulation points of surface water flows during heavy rainfall, it may be possible to propose more rational geo-disaster countermeasures for wide-area road networks.

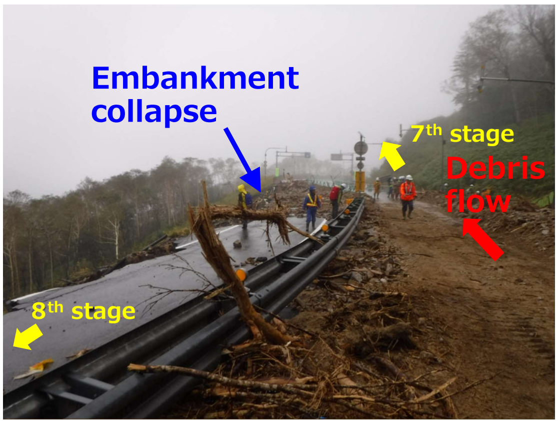

Fig. 28 Slope failure and debris flow in Nissho Pass area induced by heavy rainfall on August, 2016.

In this way, to adapt potential geo-disaster risks that are expected to occur due to climate change, it is desirable to examine about the roles of road network as the whole of road facilities toward the disaster prevention and mitigation for the unexperienced complex geo-disasters. Efforts from a new perspective different from before would have a significant implication on disaster prevention/mitigation in future.

CONCLUDING REMARKS

This study examined the case studies of two major geo-disasters mentioned above that have occurred in recent years in Hokkaido, which is a cold region vulnerable to climate change disasters. Based on the results of the case studies, this study clarified the perspectives necessary for risk assessment and disaster prevention/mitigation and discussed the direction of future academic research and technology development in addition to suggesting a possibility of new compound geo-disasters induced by the climate change. The following findings can be mainly obtained:

- The slope stability analysis considering rainfall infiltration and runoff is useful for the wide-area risk assessment of water-soil complex landslide disasters during heavy rainfalls, which are expected to increase in various parts of the world in the future due to the climate change. Since the precision of numerical simulations is considerably affected by the 3D modelling method of the topographic information, the usage of high-precision DEM data in the wide-area risk assessment of slope failure along with runoff generation is indispensable.
- Coupled model of surface flow and subsurface flow can reproduce that runoff generates when rainfall intensity exceeds the infiltration capacity of soil ground, and the slope failures caused

by runoff are successfully simulated in line with the actual phenomena. Besides, through numerical simulations using the hybrid coupled model of surface flow, subsurface flow, and soil mechanics, runoff is one of important key factors causing the slope failures during heavy rainfall, and its effects cannot be neglected.

- Flow of surface water is seriously affected by topography of catchment basin, infiltration capacity of soil ground, road alignment, shape/structure/material of pavement. Appropriate selections and combinations of these influencing factors are important for developing the rational countermeasures against runoff-induced slope failures, thus also indicating a possibility of planning the comprehensive disaster prevention and mitigation measures in terms of the design and construction for transportation infrastructures.
- Proposed slope stability analysis using the hybrid coupled model incorporating the pseudo-static method of seismic loads can appropriately evaluate the impact of seismic motion on the stress field change as well as the effect of complex interaction on the pore water pressure variation between runoff and infiltration. Accordingly, it can conduct a comprehensive wide-area slope failure simulation for the compound disasters like earthquake/rainfall induced slope failures, which would be expected to increase due to the climate change.

ACKNOWLEDGMENTS

This research was supported in part by Grant-in-Aid for Scientific Research (A) (16H02360), (Exploratory) (18K18915), and (A) (20H00266) from Japan Society for the Promotion of Science (JSPS) KAKENHI. The authors gratefully acknowledge the Hokkaido Regional Development Bureau of Ministry of Land, Infrastructure, Transport and Tourism, Hokkaido Road Management Engineering Center, Docon Co., Ltd., Prof. K. Sako, Kagoshima University, and Kagoshima prefecture for their surveyed data and comments.

REFERENCES

Babu, G.L.S., Kandhal, P.S., Kottayi, N.M., Mallick, R.B., Veeraragavan, A, 2019. Pavement Drainage: Theory and Practice, ISBN 0-81-535360-X. CRC Press.

Belfort, B., Younes, A., Fahs, M., Lehmann, F. 2013. On equivalent hydraulic conductivity for oscillation–free solutions of Richard's equation. *Journal of Hydrology*, 505: 202-217.

Bishop, A.W., 1954. The use of pore water coefficients in practice, *Géotechnique*, 4, 148-152.

Bishop, A. W. 1955. The use of slip circle in the stability analysis of slopes, *Geotechnique*, 5(1): 7-17.

Chow, V.T., 1959. Open-Channel Hydraulics, ISBN 0-07-010810-2. McGraw-Hill, New York, 572 pp.

Clement, T.P., Wise, W.R., Molz, F.J. 1994. A physically based, two-dimensional, finite-difference algorithm for modeling variably saturated flow. *Journal of Hydrology*, 161(1-4): 71-90.

COMSOL Multiphysics, 2018. Version 5.4. COMSOL Inc, Sweden.

Esteves, M., Faucher, X., Galle, S., Vauclin, M. 2000. Overland flow and infiltration modelling for small plots during unsteady rain: numerical results versus observed values. *Journal of hydrology*, 228(3-4): 265-282.

Green, W. H., Ampt, G. A. 1911. Studies on Soil Phyics. *The Journal of Agricultural Science*, 4(1): 1-24.

He, W., Ishikawa, T., Zhu, Y. 2023. Wide / narrow-area slope stability analysis considering infiltration and runoff during heavy precipitation. *Soils and Foundations*, 63(1): 101248.

Horton, R.E. 1933. The role of infiltration in the hydrologic cycle. *Eos. Transactions American Geophysical Union*, 14(1), 446-460.

Ichii, K. 2003. Optimization of design seismic coefficient based on total expected cost for gravity type quay walls. *Journal of Structural Eng./Earthquake Eng.*, JSCE, 20(1): 13-23.

Janbu, N. 1968. Slope Stability Computations. *Soil Mechanics and Foundation Engineering Report*,

Technical University of Norway, Trondheim.
Japanese Geotechnical Society (JGS). 2017. Geo-disaster report on the August 2016 Hokkaido Heavy Rainfall. Survey Team for Geotechnical Disasters in Hokkaido, Japan Induced by Heavy Rainfall on August, 2016. (in Japanese)
Japanese Geotechnical Society (JGS). 2019. Reconnaissance report on geotechnical damage caused by the 2018 Hokkaido Eastern Iburi Earthquake. Survey Team for Geotechnical Disasters in Hokkaido, Japan Induced by the 2018 Hokkaido Eastern Iburi Earthquake. (in Japanese)
Kawamura, S., Kawajiri, S., Hirose, W., Watanabe, T. 2019. Slope failures/landslides over a wide area in the 2018 Hokkaido Eastern Iburi Earthquake. *Soils and Foundations*, 59(6): 2376-2395.
Lu, N., Şener‐Kaya, B., Wayllace, A., Godt, J.W. 2012. Analysis of rainfall‐induced slope instability using a field of local factor of safety. *Water Resources Research*, 48(9).
Matsui, T., San, K.C. 1992. Finite element slope stability analysis by shear strength reduction technique. *Soils and foundations*, 32(1): 59-70.
Mononobe, N., Matsuo, H. 1929. On determination of earth pressure during earthquake. *Proc. World Engineering Congress*, Tokyo, Vol.9: 177-185.
Morgenstern, N.R., Price, V.E. 1965. The analysis of the stability of general slip surface, *Geotechnique*, 15(4): 289–290.
Mügler, C., Planchon, O., Patin, J., Weill, S., Silvera, N., Richard, P., Mouche, E. 2011. Comparison of roughness models to simulate overland flow and tracer transport experiments under simulated rainfall at plot scale. *Journal of Hydrology*, 402(1-2): 25-40.
Mukunoki, T., Suetsugu, D., Sako, K., Murakami, S., Fukubayashi, Y., Ishikura, R., Hino, T., Sugimoto, S., Wakinaka, K., Ito, S., Koyama, A. 2021. Reconnaissance report on geotechnical damage caused by a localized torrential downpour with emergency warning level in Kyushu, Japan. *Soils and Foundations*, 61(2): 600-620.
Nakanishi, H., Hamzah, M. O., Hasan, M.M., Karthigeyan, P., Shaur, O. 2019. Mix design and application of porous asphalt pavement using Japanese technology. *In IOP Conference Series: Materials Science and Engineering*, 512, 012026. IOP Publishing.
Noda, S., Uwabe, T., Chiba, T. 1975. Relation between seismic coefficient and ground acceleration for gravity-type quay wall. *Report of the Port and Harbour Research Institute*, 14(4). (in Japanese)
Okabe, S. 1924. General theory on earth pressure and seismic stability of retaining wall and dam. *Journal of Japan Society of Civil Engineering*, 10(6): 1277-1323.
Sato, A., Hayashi, T., Hayashi, H., Yamaki, M., 2017. On the geotechnical properties of decomposed granite soil in Hokkaido. *Technical Report of Hokkaido Branch of Japanese Geotechnical Society*, 57: 145–148. (in Japanese)
Simons, F., Busse, T., Hou, J., Özgen, I., Hinkelmann, R. 2014. A model for overland flow and associated processes within the Hydroinformatics Modelling System. *Journal of hydroinformatics*, 16(2): 375-391.
SoilVision, 2018. Version, 4.23. SoilVision Systems Ltd. Saskatoon, Saskatchewan, Canada.
Tan, J., Song, H., Zhang, H., Zhu, Q., Xing, Y., Zhang, J. 2018. Numerical Investigation on Infiltration and Runoff in Unsaturated Soils with Unsteady Rainfall Intensity. *Water*, 10(7): 914.
Tseng, M.H. 2010. Kinematic wave computation using an efficient implicit method. Journal of *Hydroinformatics*, 12(3): 329-338.
Yasuoka, T., Ishikawa, T., Hayashi, H., Tokoro, T., Maruyama, K., Ueno, C. 2021. Proposal of installation method of geosynthetics drainage material for frost heave depression of road pavement. *Technical Report of Hokkaido Branch of Japanese Geotechnical Society*, 61: 155-164. (in Japanese)
Zhu, Y., Ishikawa, T., Subramanian, S.S., Luo, B. 2020. Simultaneous analysis of slope instabilities on a small catchment-scale using coupled surface and subsurface flows. *Engineering Geology*, 275: 105750.
Zhu, Y., Ishikawa, T., Zhang, Y., Nguyen, B.T., Subramanian, S.S. 2022. A FEM-MPM hybrid coupled framework based on local shear strength method for simulating rainfall/runoff-induced landslide runout. *Landslides*, 19: 2021-2032.